

EVALUATION OF A CAPACITIVELY COUPLED MICROWAVE PLASMA  
ATOMIC EMISSION SPECTROMETER FOR THE DETERMINATION OF LEAD  
IN WHOLE BLOOD

By

MICHAEL WALLACE WENSING

A DISSERTATION PRESENTED TO THE GRADUATE SCHOOL  
OF THE UNIVERSITY OF FLORIDA IN PARTIAL FULFILLMENT  
OF THE REQUIREMENTS FOR THE DEGREE OF  
DOCTOR OF PHILOSOPHY

UNIVERSITY OF FLORIDA

1994

## ACKNOWLEDGEMENTS

First and foremost, my thanks go toward my parents who always supported me and never restricted me in whatever I did.

For their friendship and support, I would like to thank Cheri Morgan, Cheryl Davis, Dennis Hueber, Tye Barber, Wes Hoy, and Sophia Dixon.

Professionally, I must thank my high school chemistry teacher, Dr. MacElroy, who initially encouraged me to pursue chemistry and gave me my first "C". Drs. Harold Bell and Jim Wolfe provided me with a scholarship at Virginia Tech, kept up with my progress, and taught me how to be independent at a large university. In addition, Dr. I. C. Chu was kind enough to provide three months of industrial experience at DuPont. Finally, my professional experience was rounded out by Dr. Ben Smith and Dr. Jim Winefordner who contributed substantially to my knowledge of molecular and atomic spectroscopy.

## TABLE OF CONTENTS

ACKNOWLEDGEMENTS	ii
ACRONYM KEY	vi
ABSTRACT	viii
CHAPTER 1	
THE DETERMINATION OF LEAD IN WHOLE BLOOD	1
Introduction	1
Lead Sources	1
Lead Toxicity	2
Reference Range	4
Current Needs for the Determination of Pb in Blood	5
Potential Screening Methods	5
Atomic Absorption Approaches	8
Delves Cup Flame Atomic Absorption Spectrometry (FAAS)	8
Electrothermal Atomization - Atomic Absorption Spectrometry (ETA-AAS)	9
Anodic Stripping Voltammetry (ASV)	9
Emission Methods	11
DC Arc	11
Direct Current Plasma (DCP)	12
Inductively Coupled Plasma (ICP)	12
Conclusions	13
CHAPTER 2	
PLASMA EXCITATION SOURCES IN ATOMIC EMISSION SPECTROSCOPY	14
Introduction	14
General Plasma Parameters	14
Plasma Excitation Sources	16
Inductively Coupled Plasma (ICP)	16
Direct Current Plasma (DCP)	17
Microwave Induced Plasma (MIP)	18
Capacitively Coupled Microwave Plasma (CMP)	19

Microsampling into a Plasma . . . . .	20
Liquid Plug Techniques . . . . .	20
Electrothermal Vaporization Techniques . . . . .	21
Direct Insertion Techniques . . . . .	22
Flow Injection Analysis . . . . .	23
Conclusions . . . . .	24
 CHAPTER 3	
CAPACITIVELY COUPLED MICROWAVE PLASMA INSTRUMENTATION . . . . .	26
Introduction . . . . .	26
Magnetrons . . . . .	26
Waveguides . . . . .	27
Instrumentation Used in This Work . . . . .	34
Determination of the Optimum Length and Position of the Electrode . . . . .	46
Experimental . . . . .	46
Results . . . . .	46
Conclusions . . . . .	50
 CHAPTER 4	
THE DETERMINATION OF LEAD IN AQUEOUS SAMPLES USING	
DSI-CMP-AES . . . . .	51
General Introduction . . . . .	51
Selection of Wavelength . . . . .	51
Selection of Electrode Material . . . . .	60
Evaluation of the He Purge Time . . . . .	63
Flow Rate Optimization . . . . .	73
. . . . .	79
Power Optimization . . . . .	79
Calibration Curve . . . . .	79
Conclusions . . . . .	88
 CHAPTER 5	
THE DETERMINATION OF LEAD IN WHOLE BLOOD BY DSI-CMP-AES . . . . .	93
Characterization of Whole Blood at 405 nm . . . . .	93
Characterization of the Plasma Ashing Step using Aqueous Samples . . . . .	106
Radial and Axial Profiles . . . . .	109
Optimization of the Ashing Time . . . . .	115
Percent Recovery Study . . . . .	118
Determination of Accuracy . . . . .	125
Conclusions . . . . .	146
 CHAPTER 6	
CONCLUSIONS AND FUTURE WORK . . . . .	148
Summary of Results . . . . .	148

Future Work . . . . .	148
Nickel Cups . . . . .	148
Matrix Modifiers . . . . .	149
Feedback Regulation of the Ashing Step . . . . .	150
Other Thermal Ashing Techniques . . . . .	150
Redesign of the Plasma Torch . . . . .	150
REFERENCES . . . . .	152
BIOGRAPHICAL SKETCH . . . . .	160

## ACRONYM KEY

The acronyms that were used in this dissertation are defined below. Some of the acronyms used in this dissertation are composed of combinations of simple acronyms which have been joined by a hyphen. Only the simple acronyms have been shown below.

<u>Acronym</u>	<u>Definition</u>
AAS	Atomic absorption spectrometry.
AC or ac	Alternating current.
AES	Atomic emission spectrometry.
ALA	Aminolevulinic acid.
ALAD	Aminolevulinic acid dehydrase.
ASV	Anodic stripping voltammetry.
CDC	U.S. Centers for Disease Control (Atlanta).
CMP	Capacitively Coupled Microwave Plasma.
DC or dc	Direct current.
DCP	Direct current plasma.
DSI	Direct sample insertion.
ETA	Electrothermal atomization.
ETV	Electrothermal vaporization.
FAAS	Flame atomic absorption spectrometry.
FIA	Flow injection analysis.

FWHM	Full width at half maximum.
ICP	Inductively coupled plasma.
ID	Isotope dilution.
LC	Liquid chromatography.
MIP	Microwave induced plasma.
MS	Mass spectrometry.
NAA	Neutron activation analysis.
NHANES	National health and nutrition examination survey.
ppb	Parts per billion.
ppm	Parts per million.
ppth	Parts per thousand.
QCM	Quality control material.
RSD	Relative standard deviation.
SFC	Supercritical fluid chromatography.
TE	Transverse electric.
TM	Transverse magnetic.
TTL	Transistor-transistor logic.

Abstract of Dissertation Presented to the Graduate School  
of the University of Florida in Partial Fulfillment of the  
Requirements for the Degree of Doctor of Philosophy

EVALUATION OF A CAPACITIVELY COUPLED MICROWAVE PLASMA  
ATOMIC EMISSION SPECTROMETER FOR THE DETERMINATION OF LEAD  
IN WHOLE BLOOD

By

Michael Wallace Wensing

August 1994

Chairperson: James D. Winefordner  
Major Department: Chemistry

The determination of lead in whole blood has become of paramount importance as the Centers for Disease Control in Atlanta has recently (1991) lowered the "level of concern" for lead in blood to 10  $\mu\text{g}/\text{dL}$ . This action invalidated the most popular screening technique that was previously used, the indirect determination of lead in blood by hematofluorometry of erythrocyte protoporphyrin, which cannot determine lead at levels below 25  $\mu\text{g}/\text{dL}$ .

This work evaluated the use of a capacitively coupled microwave plasma atomic emission spectrometer for the determination of lead in whole blood (CMP-AES). This CMP-AES incorporated a tungsten wire electrode which was used both to support the plasma and to hold the sample. The sample was deposited on the electrode and dried at low microwave powers. Following this, a low-power helium plasma was ignited and



allowed to ash the sample. Finally, the power was increased which resulted in the atomization and excitation of lead. The resulting lead emission was detected as a transient signal using a monochromator and a photodiode array detector. Such a device improves upon other atomic emission devices as 100% of the sample was transferred into the plasma. Detection limits as low as 0.6 ppb (3 pg Pb) were determined for aqueous samples with a precision better than 10%. Detection limits as low as 4 ppb (20 pg Pb) were obtained for lead in whole blood with a precision of 16 % at concentrations as low as 80 ppb. These detection limits rival those of electrothermal vaporization atomic absorption spectrometry, and are better than those obtained by inductively coupled plasma atomic emission spectrometry.

## CHAPTER 1 THE DETERMINATION OF LEAD IN WHOLE BLOOD

### Introduction

Lead is abundant in the environment, originating mostly from industrial sources.<sup>1</sup> It is not essential for the human body and has no beneficial role.<sup>1</sup> At high concentrations, it is toxic. Adults are less susceptible to the effects of lead poisoning than children. Lead poisoning is silent as symptoms of lead poisoning are not readily discernable. Although a massive effort had been launched by the U.S. and other countries of the world to reduce lead exposure<sup>2</sup>, it has recently been realized that lead is toxic at lower concentrations than was previously thought.<sup>1</sup> Therefore, further reduction to lead exposure is necessary.

Blood screening methods are used to determine an individuals exposure to lead. Considering that the level of concern for lead in blood has been lowered<sup>1</sup>, more sensitive methods need to be developed. Potential new screening methods are under evaluation.<sup>3</sup> The goal of the research in this dissertation was to evaluate one potential method for the evaluation of lead in blood.

### Lead Sources

Industrial sources are the major source of lead exposure, and the atmosphere is the major route of contamination. Anthropogenic activities transfer 700 times more lead into the environment than natural causes.<sup>4</sup> The total emission of lead into the

atmosphere in 1983 was estimated to be between  $7 \times 10^8$  and  $19 \times 10^8$  kg/yr and was based on emission studies of Western Europe, the U.S., Canada, and the Soviet Union.<sup>5</sup> Since pollution control efforts are less stringent in third world countries, this number likely underestimates the total emission.

A considerable amount of lead has been removed from the environment due to several factors. These include the elimination of lead from gasoline (1992), the voluntary removal of lead solder from food cans by the food canning industry, and the banning of the addition of lead to residential paint in 1978 by the Consumer Product Safety Commission.<sup>2</sup>

Some remaining sources of lead contamination are old paint, soil along old highways, water that has come into contact with lead soldered plumbing connections, improperly fired ceramics, and improperly fired leaded glass.<sup>6</sup>

#### Lead Toxicity

The U.S. Centers for Disease Control (CDC) currently considers the "level of concern" for lead in blood to be 100 ppb.<sup>1</sup> This was recently (1991) lowered from the previous "level of concern", 250 ppb.<sup>1</sup>

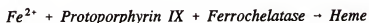
Lead shows several toxic effects. Some of these are the reduction of red cell production, the reduction of globin synthesis, and the inhibition of heme production.<sup>7</sup> The inhibition of heme production can have severe consequences and is discussed. The human body makes use of enzymes to carry out chemical reactions. Lead inhibits the production of many of the enzymes which are involved in the production of heme. Heme is the functional group of hemoglobin which is responsible for oxygen binding. Lead

inhibits the production of *δ-aminolevulinic acid dehydrase (ALAD)*. The chemical reaction that would take place in the absence of lead is:<sup>7</sup>



This results in the buildup of *δ-aminolevulinic acid (ALA)* in an individual's blood and urine. The detection of *ALA* in urine was used once as a screening test for Pb. However, blood lead concentrations must reach 400 ppb before the urine *ALA* concentration increases. This test is too insensitive to meet the current requirements set by the CDC.

Lead also inhibits the production of *ferrochelatase*. This enzyme catalyzes the incorporation of iron into the porphyrin ring of *protoporphyrin IX*. The reaction is shown below:<sup>10</sup>



The inhibition of *ferrochelatase* production results in the accumulation of *protoporphyrin IX* in the erythrocyte. The measurement of *protoporphyrin IX* was previously the most popular screening technique for determining the Pb concentration in blood<sup>3</sup>; however, the recent lowering of the "level of concern" for Pb in blood has invalidated this technique.

Another effect associated with lead poisoning is the accumulation of coproporphyrin in erythrocytes. This buildup of coproporphyrin can be measured in

urine. However, increases in urine concentrations of coproporphyrin do not occur until an individual has a blood lead concentration of 400 ppb.<sup>8</sup>

Lead poisoning at concentrations below 100 ppb has resulted in low IQ's, impaired hearing, and impaired growth in children, while lead poisoning at concentrations between 100 ppb and 200 ppb has resulted in impaired vitamin D metabolism and have lowered nerve conduction velocity. Lead concentrations above 400 ppb have resulted in reduced hemoglobin synthesis and anemia; above 500 ppb, colic, frank anemia, and encephalopathy have resulted. Levels above 1 ppm have resulted in death.<sup>9</sup> Treatment for individuals with very significant blood lead levels (> 450 ppb) involves the use of chelating agents which bind lead and are excreted.<sup>10</sup> These chelating agents are administered orally, intramuscularly, or intravenously.

#### Reference Range

The average whole blood lead concentrations have been falling as lead pollution has decreased. A national study (NHANES II) showed that average blood lead levels of U.S. adults decreased from 160 ppb in 1976 to 95 ppb in 1980.<sup>11</sup> These years corresponded to the phasing out of lead in gasoline. Recent analyses have shown that this level has further decreased. A 1993 U.S. study which included 100 adults determined the average lead concentration was 30 ppb. The reference range was 3 - 131 ppb.<sup>12</sup> Since an average value has little meaning when applied to an individual, a "reference range" is determined. This requires reporting the range of concentrations obtained after the lowest 2.5 % and highest 2.5 % concentrations associated with the population have been removed. A study performed in Italy in 1989 on 959 adults

reported a mean concentration of 158 ppb.<sup>13</sup> The reference range associated with this data was 40 - 256 ppb. It is clear that the variation in the blood Pb level from one individual to the next is large. Also, the average blood lead level varies substantially with geographic location.

#### Current Needs for the Determination of Pb in Blood

Any screening technique must meet the following requirements: the total analysis time must be short, the cost per sample must be low, the instrument should be simple to operate, and the method should be accurate and precise. Also, when dealing with biological samples, the amount of sample needed must be small. In addition, the method should be accurate and precise. The CDC has set up several requirements for a lead in blood screening method. The time per analysis must be less than 5 minutes; the sample size must be less than 200  $\mu$ L. Also, the method should yield a result which is within 10% of the true value. Replicate measurements must be within 10% as given by the % RSD, and the detection limit must be below 20 ppb.

Any method which is used to determine an element that is present in blood at ppb levels must be extremely selective. Carbon, hydrogen, nitrogen, and oxygen make up 96% of man. In addition, the essential elements are found in man at much lower quantities and are shown in Table 1-1.<sup>14</sup> Several other elements are present in blood, also. All of these need to be discriminated against when determining lead.

#### Potential Screening Methods

Several approaches have been used to determine lead in whole blood: isotope dilution mass spectrometry (ID-MS),<sup>15</sup> neutron activation analysis (NAA),<sup>16</sup> inductively

Table 1-1: Essential Elements in Man

Element	Abundance (ppth)*
Ca	15
K	10
S	2.0
K	2.0
Cl	1.5
Na	1.5
Mg	0.50
Fe	0.059
Zn	0.033
Cu	0.0014

\*ppth = parts per thousand

coupled plasma mass spectrometry (ICP-MS),<sup>17</sup> inductively coupled plasma atomic emission spectrometry (ICP-AES),<sup>18</sup> microwave induced plasma atomic emission spectrometry,<sup>19</sup> electrothermal atomization atomic absorption spectrometry (ETA-AAS),<sup>20</sup> flame atomic absorption spectrometry (FAAS)<sup>21</sup> and anodic stripping voltammetry (ASV)<sup>22</sup>. However, all the mass spectrometry approaches and the neutron activation analysis approach, while valid, are too expensive to be used as a screening technique. This leaves the approaches of FAAS, ASV, ETA-AAS, and the plasma emission techniques to be considered.

#### Atomic Absorption Approaches

Atomic absorption spectrometry is a very sensitive and selective approach when a line source is used as the radiation source. Problems associated with this technique are due to the great amount of light scattered off of vaporized particles. Good background correction is necessary in order for reliable results to be obtained.

#### Delves Cup Flame Atomic Absorption Spectrometry (FAAS)

In the Delves cup method, the sample is added to a nickel crucible. Ashing of the sample either takes place on a hot plate, or using the heat from the flame. A large number of samples can be pretreated using a hot plate, making Delves cup AAS useful in clinical applications. A multi-slot burner is used to support the flame. A quartz atomic absorption cell is held 2 cm above the burner head. The quartz cell has a small centrally located hole. The sample is introduced between the burner head and the cell. Volatilization of the sample occurs when the crucible is introduced into the flame, and the atoms are captured in the quartz cell. Delves cup AAS is very sensitive and has a



detection limit around 1 ppb Pb. This method requires only a small amount of sample (100  $\mu$ L). In addition, the method is very rapid. However, Delves Cup AAS determinations are not very precise, and all measurements are usually done in triplicate.

#### Electrothermal Atomization - Atomic Absorption Spectrometry (ETA-AAS)

In ETA-AAS, the whole blood sample is usually diluted 10:1 with Triton X-100, a surfactant, and a matrix modifier which contains phosphate to convert Pb to lead phosphate. Ten microliters of sample are typically deposited in the atomizer. The atomizer goes through its typical stages of drying, ashing, atomization, and cleanout. This technique is the most popular method for the determination of lead in whole blood. It is not without problems, however. The buildup of carbonaceous residues have been reported.<sup>23</sup> Also, good background correction techniques, such as the use of Zeeman background correction<sup>24</sup>, are necessary in order to correct for the intense scattering as the blood particles are vaporized. Zeeman background correction is preferred over the deuterium arc lamp method. The disadvantage of using Zeeman background correction is its fairly high cost.

ETA-AAS is also very sensitive. Detection limits around 10 ppb are achieved. The precision is around 5 %.<sup>25,26</sup> The total analysis time is approximately 2 minutes per sample. Matrix-matched standards are necessary for the most reliable results, although calibration using aqueous standards have been reported.<sup>27,28</sup>

#### Anodic Stripping Voltammetry (ASV)

ASV has come a long way in the rapid detection of lead in whole blood. In ASV the analyte is preconcentrated on the working electrode by moving the electrode to a

negative enough potential to reduce the analyte and stirring the solution to speed up the deposition process. This is known as the pre-electrolysis step. After the pre-electrolysis step, the potential is stepped incrementally to less negative values, stripping the analyte from the electrode. Each electrochemical species is removed at its characteristic stripping potential. The working electrode is typically composed of a thin film of mercury which has been deposited on a glassy carbon substrate.<sup>29</sup>

Commercial analyzers are now available to determine lead in blood such as the ASV Trace Metal Analyzer (Environmental Sciences Associates, Bedford, MA); 100  $\mu$ L of whole blood is added to a plastic tube which contains 2.9 mL of a metal exchange reagent, commercially known as Metexchange® (Environmental Sciences Associates, Bedford, MA). This metal exchange reagent contains 10.7 g chromium chloride, 14.3 g calcium acetate, 28 mg of mercuric ion per liter of solution as well as surfactant and acids. The surfactant and the acids are used to digest the sample, the calcium acetate provides a buffer solution, and the chromium chloride provides an electrolytic solution. The analysis is carried out in the same plastic tube. The total analysis time is approximately 3 minutes. In addition, a 1-minute cleanup step is also required, to ensure that all Pb is removed from the electrode. Potential interferents include tin, thallium, and copper. Copper is the worst interferent. Elevated copper levels are found in the blood of pregnant women. The precision of the method is about 10 %, and the detection limit is below 20 ppb. This method takes more time than ETA-AAS and is more prone to memory effects. In addition, the precision is worse than the precision in ETA-AAS.

The massive dilution factor, a factor of 30, makes the potential for sample contamination greater for ASV than for ETA-AAS.

### Emission Methods

At least four types of plasmas have been investigated concerning the determination of lead in whole blood, the DC arc, the Direct Current Plasma (DCP), the Inductively Coupled Plasma (ICP), and the Microwave Induced Plasma (MIP). All require rather large amounts of sample (in the mL range) and either sample preconcentration or introduction by electrothermal vaporization.

### DC Arc

Troshkova and Yudelevich<sup>30</sup> required a 2 mL sample of whole blood. They preconcentrated the lead by extracting it with a fairly specific chelating agent, polyarsenazo. This chelating agent sorbed 99.99 % of the Pb and only 0.1 % of the Na and Ca. The sample size and the analysis time was far too laborious to be used as a screening method.

The same authors<sup>31</sup> have also tried removing Na, K, and Fe from blood serum using dibenzo-18-crown-6 in  $\beta,\beta$ -dichlorodiethyl ester. Then, they preconcentrated the blood serum to determine Pb.

Marinov<sup>32</sup> tried to reduce the sample preparation, and instead optimize the plasma excitation process. Blood serum was studied. The sample was dried in the electrode crater. The sample was spiked with 200 ppb Pb. 200  $\mu$ L of serum was deposited in the crater, and dried. The precision varied from 4 to 14%.

### Direct Current Plasma (DCP)

According to Schramel<sup>33</sup>, neither the DCP or ICP are sufficiently sensitive to determine Pb when whole blood is introduced through a nebulizer. In order to ensure that the nebulizer did not clog, a surfactant would have to be added to lower the viscosity of blood, resulting in further dilution.

### Inductively Coupled Plasma (ICP)

van Deijck *et al.*<sup>34</sup> agree with Schramel<sup>33</sup> that the ICP is not sufficiently sensitive to determine lead in whole blood without preconcentration. van Deijck *et al.*<sup>34</sup> evaluated several sample treatment procedures. They determined that Fe was a major interferent when Pb was determined at 220 nm. This Pb transition is the most sensitive emission transition in an ICP. A 500 ppm Fe signal was equivalent to a 200 ppb Pb signal. Therefore, it was desired to remove the Fe from the whole blood, by extraction with amyl acetate. In addition, a preconcentration step was performed.

The sample treatment was as follows: A 5 mL aliquot of whole blood was dried in an oven overnight. Following this, the samples were digested with activated oxygen in a microwave digestion chamber for 24 h. The ash was dissolved in concentrated HCl. Iron was then separated by diluting one volume of the digested sample with 2 volumes of n-amyl acetate; 99 % of the Pb remained in the concentrated HCl layer, while 99% of the Fe was extracted into the n-amyl acetate layer. The HCl layer was retained for further analysis. 8-hydroxyquinoline was then packed into a glass column and used to preconcentrate the Pb. Since 8-hydroxyquinoline does not bind K, Na, Mg, and Ca well, 65 % of these species were removed. The sample pH was adjusted to 8, and the now

basic Pb solution was pumped through the glass column. After the column was washed, the Pb was removed from the column with 1 mL of a 1 M HCl solution; a 100  $\mu$ L aliquot of this sample was added using an injection valve into a normal stream of liquid flowing into a nebulizer. Most of the matrix constituents had been removed by this point, and the total preconcentration factor was 5. Certified whole blood standards were analyzed containing 410 and 735 ppb lead, respectively. The method was accurate at these concentrations, although certainly the method was very laborious. Further preconcentration could be accomplished by evaporating the 1 mL washing off the column to 100  $\mu$ L, resulting in a preconcentration factor of 50.

### Conclusions

The determination of lead in blood is very challenging. The CDC has made it even more challenging by further lowering the "level of concern" for lead in blood. The most reliable method at present for the determination of lead is ETA-AAS, followed by ASV. Emission methods are much more laborious.

## CHAPTER 2

### PLASMA EXCITATION SOURCES IN ATOMIC EMISSION SPECTROSCOPY

#### Introduction

This chapter introduces the various parameters which affect the analytical determination of an element with plasma atomic emission spectroscopy. Those factors which control the stability of a plasma source and, therefore, the precision of the method, the sensitivity of the plasma emission method, and other figures of merit are discussed. The different forms of atmospheric pressure plasmas are described along with their advantages and disadvantages. In addition, alternative sample introduction techniques are described as conventional nebulization techniques cannot be used in the determination of lead in a viscous sample such as blood.

#### General Plasma Parameters

There are several parameters which effect the sensitivity of an analytical determination using atomic emission spectrometry. In the most common emission methods, solutions are nebulized into a plasma. The sample transport efficiency is determined by the characteristics of the nebulizer. An ultrasonic nebulizer is the most efficient nebulizer, being 5 - 10 % more efficient than a conventional pneumatic nebulizer. After the sample is nebulized, it is brought into the spray chamber which may be heated to produce a dry aerosol; alternatively, a wet aerosol may be brought into the plasma. Low power plasmas require dry aerosols, while wet aerosols can be introduced

into higher power plasmas. Once the wet aerosol is introduced into the plasma, it must be desolvated. If the sample introduction rate is too great, the plasma will be extinguished as there is not enough energy to desolvate the particles and to sustain the plasma. In most plasmas the sample introduction rate which permits a stable plasma is below 1 mL/min. Following desolvation, the sample is volatilized and atomized. Refractory compounds require more energy to be decomposed than non-refractory compounds. If the plasma temperature is too low, selective volatilization will occur. For example, the plasma temperature may be sufficient to determine lead in the form of lead chloride but not lead in the form of lead phosphate, and speciation errors will occur. In addition, the plasma must have a sufficient temperature to decompose the compound to be studied; otherwise, selective atomization will occur. The higher the plasma gas temperature, the more insensitive the plasma is to these problems, although selective volatilization and atomization occurs to a certain extent in all plasmas. Once the atoms are formed, they are excited in the plasma; and, if the excitation temperature of the plasma is sufficiently high, emission will result. Since the excitation temperature of plasmas is higher than the gas temperature of the plasma, the plasma is not in thermodynamic equilibrium. In general, the greater the ionization potential of the plasma gas, the greater the excitation temperature of the plasma, ( $\text{He} > \text{Ar} > \text{N}_2$ ).<sup>35</sup> In addition, the sensitivity of the determination is affected by the residence time of the sample in the plasma. Longer residence times result in more efficient atomization of the compounds, and also more intense emission, and may be obtained with lower gas flow rates.

### Plasma Excitation Sources

#### Inductively Coupled Plasma (ICP)

The inductively coupled plasma is the most popular plasma excitation source used today.<sup>3,36</sup> The plasma torch consists of three concentric tubes, which are designated as the "inner gas tube or carrier gas tube," the "intermediate tube," and the "outer tube."<sup>37,38,39</sup> Encircling the tube is a two- or three-turn induction coil which is referred to as the load coil. Gases are introduced to the tube, and radio-frequency energy is applied to the coil. The load coil produces a strong oscillating magnetic field perpendicular to the load coil axis. This magnetic field induces an electric field in the coil region. The plasma is "seeded" with electrons produced from a Tesla coil. If the magnetic field produced is sufficiently strong, a plasma will form. The temperature produced inside the load coil is approximately 10,000 K,<sup>40</sup> so a vortex gas flow carried through the outer tube is necessary in order to keep the quartz torch from melting.

The sample is introduced via the inner tube as an aerosol. The sample is desolvated, atomized and excited as it travels through the plasma from the load coil to the viewing region, typically 12 - 18 mm above the load coil, where the temperature is approximately 5000 K. The residence time of atoms in the plasma depends on the carrier gas flow rate (0.5 - 1 L/min) and is typically 2 ms, which is a 2 x greater than the residence time of an atom in a combustion flame. This is due to the inert nature of the plasma. Because the temperature of the ICP is much greater than the temperature of a flame, even refractory elements are decomposed.<sup>41</sup>



Most ICP's operate at a power of 1-2 kW, although powers as high as 7 kW<sup>42,43</sup> have been used. The operating frequency of the plasma is either 27 MHz or 40 MHz. The 40 MHz frequency is preferred due to the greater plasma stability and the lower background which is observed at this frequency. ICP's typically operate with an outer gas flow of 15 - 20 L/min Ar, an intermediate gas flow of 0 - 1 L/min Ar and a carrier gas flow of 0.5 - 1 L/min Ar.<sup>44</sup>

#### Direct Current Plasma (DCP)

The modern versions of DCP's consist of three electrodes.<sup>45</sup> Two anodes composed of graphite are spaced at equal distances below a cathode. The cathode is composed of thoriated tungsten. The three electrodes form a triangular structure, the top vertex being the cathode and the two lower vertices, the anodes. All the electrodes are surrounded by ceramic sleeves through which Ar is introduced tangentially. A discharge forms between the cathode and the two anodes, which results in an inverted "Y" shaped plasma - the two anodes are tilted 30 degrees to make the bottom of the inverted "Y". Sample is introduced as an aerosol between the two anodes through a wide sample introduction tube, and emission is viewed just below the triangular region formed by the inverted "Y" of the arc, where the temperature of the plasma gas is constant and between 5000 K and 6000 K. The precision of the DCP method is between 0.5 and 1%, and the power requirements are lower than that of the ICP, for only 700 W is required. The total Ar consumption is reduced compared to an ICP as the Ar flow rate for the anodes and the cathode is between 1.2 - 1.5 L/min, each. The flow rate for the nebulizer is 4-6 L/min. Therefore, the total argon consumption ranges from 6 to 9 L/min. The

background emission of the DCP is lower than that of the ICP, as fewer strong Ar lines are observed, and the solution uptake is greater than that of the ICP (2-3 mL/min).<sup>46</sup>

#### Microwave Induced Plasma (MIP)

Modern microwave induced plasmas (MIPs) utilize a Beenakker cavity which inductively couples microwaves to the plasma.<sup>47,48,49,50</sup> The function of the Beenakker cavity is to support a standing microwave. Microwave energy (2450 MHz) is supplied to the cavity via a coaxial cable. The plasma torch is axially positioned in the center of the cylindrical Beenakker cavity, and argon is introduced through the central channel of the torch. The cavity is seeded with electrons from a tesla coil, and if the microwave power is sufficiently strong a plasma will ignite at the tip of the quartz torch. The sample is introduced as an aerosol through the central channel of the quartz torch. The carrier gas flow rate is typically 1 L/min. The plasma gas is typically Ar or He, although N<sub>2</sub> has also been used. The sample introduction rate is below 1 mL/min, and the viewing position is 1 - 2 mm above the cavity. Most MIPs are viewed axially, looking end on into the plasma rather than from the side since better detection limits are obtained in the axial viewing mode.

The powers utilized range from below 100 W<sup>51</sup> to 1.6 kW<sup>52,53</sup>. Low power MIPs have low kinetic energy and low plasma gas temperatures (1000 to 2500 K), which are insufficient to dissociate thermally stable compounds. Aqueous samples cannot be injected into MIP cavities without desolvation when the applied power is below 300 W.<sup>54</sup> When higher powers are used, the cavity heats up as microwave losses become severe, and tuners are required to impedance match the Beenakker cavity and the

generator. MIPs below 120 W have been used primarily as emission detectors for gas chromatography eluates.<sup>55,56,57</sup> Moderate power MIPs (500 W), have been used as emission detectors for directly introduced coal samples,<sup>58</sup> and also for liquid chromatography (LC)<sup>59</sup> and supercritical fluid chromatography (SFC) eluates.<sup>60</sup> A 1.6 kW plasma has been used to measure metals and nonmetals in aqueous solutions.<sup>61,62,63</sup>

#### Capacitively Coupled Microwave Plasma (CMP)

Capacitively Coupled Microwave Plasmas (CMPs) of the type reported in this dissertation utilize an electrode which is supported by the central tube of the discharge tube to support a plasma. Microwaves are generated by a magnetron which is capacitively coupled to a short-circuited rectangular waveguide. The electrode is also capacitively coupled to this waveguide. Either a tesla coil can be used to initiate the discharge, or the plasma may be allowed to autoignite. This auto-ignition feature is a unique feature of the CMP, as the electric field strength generated near the electrode tip is much greater than that generated in the MIP or the ICP. Sample is introduced usually as an aerosol via the inner tube of the torch at typically 1 - 1.5 mL/min. In order for the aerosol to pass through the electrode, a small 1 mm diameter hole is drilled axially through the electrode. Flow rates ranging from 1 to 20 L/min are typically used, and either He or Ar is used as the plasma support gas.

The design of the CMP cavity can be credited to Cobine and Wilbur<sup>64,65</sup> and Schmidt<sup>66</sup>. Mavrodineau and Hughes<sup>67</sup> were the first to apply a CMP to the measurement of species in solutions. They reported a gas temperature of 2900-3300 K

in both a He and a H<sub>2</sub> discharge. Similar plasma temperatures have also been observed in a 700 W He plasma (3000 K).<sup>68</sup> Kessler applied the CMP to the determination of glasses.<sup>69</sup> The analysis of steels has also been reported.<sup>70,71</sup>

The gas temperatures decrease in the following order: ICP > DCP > CMP > MIP. Therefore, the atomization efficiency of the ICP is greater than that of any other plasma, and the ICP as a result is the most free from matrix effects. However, the excitation efficiency of the CMP and the MIP, when helium is used, is higher than that of the ICP. As a result the analysis of refractory compounds, is favored by the ICP; however, the analysis of difficult to excite species such as nonmetals is favored by the CMP or MIP.

#### Microsampling into a Plasma

With conventional nebulizers the smallest volume of sample which can be nebulized into a plasma is 1 mL. This sample size is too large for the analysis of biological materials. Several microsampling techniques have been studied and include liquid plug techniques, electrothermal vaporization techniques, direct insertion techniques, flow injection analysis, and liquid chromatographic techniques. Since speciation information is not required or desired in the determination of lead in whole blood, liquid chromatographic techniques will not be discussed.

#### Liquid Plug Techniques

Liquid plug techniques involve coupling a micropipet to a pneumatic nebulizer. Sample uptake is either unassisted, utilizing aspiration only to draw sample into the nebulizer, or assisted utilizing a peristaltic pump to force more viscous liquids into the

nebulizer. The detection limits for liquid plug techniques are 2 - 10 times worse than continuous nebulization.<sup>72</sup> The use of an internal standard has been observed to improve the precision in the measurement of elements in serum and whole blood.<sup>73</sup>

### Electrothermal Vaporization Techniques

Electrothermal vaporization (ETV) techniques make use of an electrically heated element where the sample is deposited, volatilized and carried into the plasma using a carrier gas. The heating element is composed of graphite, nickel, tungsten, tantalum, or platinum and is in the form of a rod, cup, boat or filament. Electrothermal vaporizers are advantageous as the sample can be ashed prior to introduction in the plasma. If the analyte is less volatile than the matrix or can be made so with the use of a matrix modifier, the matrix can be selectively removed from the analyte prior to the volatilization of the analyte. The utilization of ETV techniques results in a more stable plasma and a simplified emission spectrum. Electrothermal vaporization provides detection limits which are 1 - 2 orders of magnitude better than continuous nebulization.

Electrothermal vaporization into a plasma was first performed by Kleinman and Svoboda<sup>74</sup>, who heated a graphite disk to volatilize a sample into an electrodeless discharge. A graphite rod vaporizer and ICP were used by Kirkbright and coworkers, and transport efficiencies as high as 60 % were obtained.<sup>75,76,77,78,79,80</sup> Ng and Caruso deposited 5 and 10  $\mu\text{L}$  aliquots into a pyrolytically coated carbon cup vaporizer in the analysis of seawater and organic solutions in an ICP.<sup>81,82,83,84</sup> A Pyrex cup was used by Masuda and coworkers<sup>85</sup> for the discrete introduction of 20 - 40  $\mu\text{L}$  samples and osmium was measured. Nixon and coworkers<sup>86</sup> used a tantalum strip

vaporizer for discrete sample introduction into an ICP, while Kitazume<sup>87</sup> used a platinum or tungsten filament placed in a very small 4.5 mL chamber to vaporize samples into an ICP and obtained excellent detection limits, even for ETV.

Conventional furnaces which are normally used for ETA-AAS have also been coupled to a plasma. An internal standard was observed to increase the precision of the technique by 40%.<sup>88,89</sup> Tikkannen and Niemczyk<sup>90</sup> have controlled the heating rate of an ETV in order to thermally separate compounds of different volatilities in time, and this resulted in minimized spectral interferences. Peak area has been reported to be more reliable than peak height in ETV-AES. The measurement of peak area is independent of the heating rate, while the measurement of peak height is not.<sup>91</sup> Dean and Snook<sup>92</sup> analyzed the process of atom condensation which occurs above the graphite rod in an ETV. They observed that more volatile atoms persist as atoms for a longer distance and are adsorbed or react with surfaces more quickly. Therefore, design considerations are important in an ETV.

#### Direct Insertion Techniques

Direct insertion techniques utilize an electrode which also holds the sample. This sample is dried on the electrode and then brought into contact with the plasma, where the sample is atomized and excited. Salin and Horlick<sup>93</sup> were the first to carry out this technique. They deposited 5  $\mu$ L aliquots onto the electrode. This electrode was inserted in the injector tube (inner tube) of an ICP torch and raised to the ICP load coil, where the sample was dried inductively at a low RF power. The electrode was subsequently lowered, the ICP ignited, and the electrode was raised into the plasma. Detection limits

which were a factor of 10 lower than conventional nebulization were reported. Kirkbright and Sargent used a graphite electrode in much the same way, although the sample was dried with a heat gun before it was inserted into the continuously running ICP.<sup>94,95</sup> In order to improve the precision of this technique, Li-Xing *et al.*<sup>96</sup> used a computer controlled stepper motor to control the positioning of the electrode. A further automated system utilized graphite cups which were raised under computer control. A robot was used to exchange graphite cups. The best precision was obtained with this technique.<sup>97</sup>

#### Flow Injection Analysis

In flow injection analysis (FIA), the sample is introduced into a carrier stream which transports the sample to the plasma. This technique requires a sampling valve, peristaltic pumps and plastic tubing. Chemical reactions, electrochemical reactions and simple dilutions may be carried out between the point of injection and the introduction of the sample into the plasma. Sample sizes are approximately 100  $\mu\text{L}$ , and high sample throughput is possible. As the technique is highly automated, operator error is minimized. Greenfield<sup>98,99</sup> and Gallego *et al.*<sup>100</sup> have commented on the possibilities of coupling FIA methods with emission detection.

Blood serum was analyzed using FIA by injecting 20  $\mu\text{L}$  samples into the carrier gas stream, these samples were diluted 1:1 to avoid matrix effects.<sup>101</sup> A high solids nebulizer was used to introduce the diluted blood into the plasma. Several parameters have been studied in FIA, including the flow rate, the total injected volume and the mixing coil length.<sup>102</sup> For calibration purposes, the standard additions technique is

easily automated with FIA.<sup>103,104</sup> Also, the addition of external standards for increased precision is also easily automated with FIA.<sup>105</sup> Preconcentration techniques have been utilized in conjunction with FIA. Long and Snook<sup>106</sup> used an electrochemical cell to selectively deposit the analyte onto a glassy carbon electrode. After the matrix was removed, the analyte was stripped from the electrode and back into the carrier stream. Other workers have utilized anodic stripping voltammetry to preconcentrate analyte on the electrode and minimize matrix effects before introducing the sample into the plasma.<sup>107</sup> Hydride generation has also been performed in conjunction with FIA<sup>108</sup> and is important, as it offers a way of selectively removing lead from the blood matrix. Thirty elements including Pb have been determined simultaneously in human serum using ICP-AES with hydride generation.<sup>109</sup> Detection limits for FIA are better than conventional pneumatic nebulization techniques; however, the extent of improvement depends on the methods that are coupled with the FIA system.

### Conclusions

Several characteristics affect the performance of an atomic emission method. These include the power of the plasma, the plasma gas used, the plasma gas flow rate and the plasma gas temperature. The ICP has the highest plasma gas temperature of any of the plasmas; however, the excitation temperature of this plasma source is low compared to the CMP and the MIP.

Several methods have been used to introduce samples into a plasma. Due to the low concentration of Pb typically found in blood and due to the viscous nature of blood, conventional nebulization techniques cannot be used. Alternative methods such as plug



injection, electrothermal vaporization, discrete sample introduction or flow injection analysis must be used. Plug injection offers no way of removing the sample matrix, while electrothermal vaporization and discrete sample introduction rely on selective volatilization of the matrix. The two latter techniques require very little sample treatment, thus the possibility of sample contamination is greatly reduced. FIA offers the advantages of chemical/electrochemical removal of the blood matrix and the selective preconcentration of the analyte. However, since more reagents are used in FIA and since the sample is processed more than in electrothermal vaporization or discrete sample introduction, the possibility of sample contamination is greater. The work in this dissertation uses a technique which involves discrete sample introduction into a CMP. Discrete sample introduction is simplified in a CMP since it is the only plasma which uses an electrode to support the plasma. The sample may be deposited directly onto the electrode, ashed with a low power plasma utilizing the selective volatilization feature of low power plasmas to thermally remove the matrix, and atomized and excited by increasing the plasma power. Since the electrode is stationary in a CMP, precision should be enhanced over DSI methods which rely on reproducible positioning of the electrode to obtain acceptable precision. As in DSI, transfer of the sample into the plasma should be effectively 100 %, and a low detection limit for lead should be obtained.

## CHAPTER 3 CAPACITIVELY COUPLED MICROWAVE PLASMA INSTRUMENTATION

### Introduction

In order to work with microwave plasmas most efficiently, several concepts concerning microwave devices need to be understood. Theory is presented in this chapter about magnetrons (microwave sources), waveguides, and the efficient coupling of microwaves to a plasma through a waveguide. Following this, the instrumentation used in this work is described, and the optimum position and length of the electrode necessary for optimum coupling to the waveguide are determined.

### Magnetrons

Magnetrons (M-type crossed field devices) are the most commercially available form of microwave tubes, and consequently the most used in plasma research. Most emit at 2.45 GHz, and produce microwave powers from 100 W to 3000 W. They consist of a negatively biased circular cathode which is surrounded by a circular anode. The cathode produces electrons through thermionic emission of a heated tungsten wire. These electrons would normally travel straight toward the anode; however, a perpendicular magnetic field provided by a permanent magnet is applied which keeps the electrons moving in a curved path. In the presence of a constant magnetic field, there is a potential at which the electrons will barely graze the anode before returning to the

cathode. This is known as the Hull potential, and is used for microwave operation.<sup>110,111,112,113</sup> Magnetrons are nonlinear diode-like devices. Similar to all diode devices, the most stable operation results when the magnetron current is regulated, rather than its voltage.<sup>114</sup>

### Waveguides

Conventional transmission lines such as coaxial cable are very inefficient at microwave frequencies (0.4 to 300 GHz). There are three major types of losses that occur within a transmission line: ohmic, dielectric, and radiational. Ohmic losses are greater at higher frequencies because ac currents are carried only on the surface of a conductor while dc currents are carried throughout the whole conductor. This loss becomes very important at microwave frequencies. At the critical depth ( $\delta$ ), also known as the depth of penetration, the current density decreases to  $1/e$  of its surface value. The critical depth is related to the frequency by

$$\delta = \sqrt{\frac{1}{2\pi\nu\sigma\mu}}$$

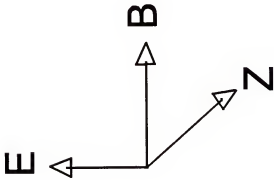
where  $\sigma$  = the conductivity of the transmission line in mhos/meter,  $\mu$  = the permeability in Henrys/meter, and  $\nu$  = the frequency, in Hz.<sup>115</sup> Therefore, a 2 mm diameter gold wire is approximately 455 times more conductive at dc frequencies, than at 2.45 GHz. Other losses that occur in transmission lines are dielectric losses which occur as the electric field of the conductor causes molecules within the insulator to oscillate, transferring energy into the insulator which is heated. Also, radiative losses are result as the electromagnetic wave propagates away from the surface of the conductor. Because

of these losses, the power sent through a coaxial cable must be kept to a minimum, otherwise the cable will overheat. Waveguides are much more efficient at transmitting energy at microwave frequencies.

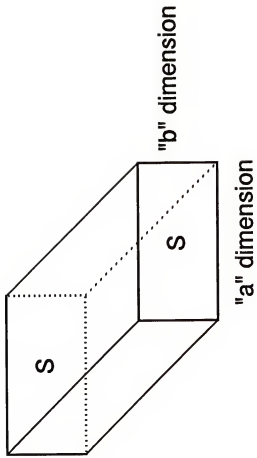
The waveguide is a resonant cavity.<sup>116</sup> Its main function is to transfer the energy from the magnetron to the electrode with minimal losses. The energy input into a waveguide propagates as an electromagnetic wave through an air dielectric, and not as a current through a wire. Therefore, the ohmic losses are minimal. The ohmic losses that do occur as the electromagnetic wave interacts with the walls of the waveguide are minimized by constructing the waveguide of materials of low resistivity. Waveguides are usually constructed of brass, aluminum, or copper and are sometimes coated with a few micrometer thick layer of gold or silver.<sup>117</sup>

Only two modes of propagation satisfy the boundary conditions imposed by a waveguide, the transverse electric (TE), and transverse magnetic (TM) modes. The boundary conditions of a waveguide require that the electric field be orthogonal to the conductor in order to exist at the surface of the conductor, and that the magnetic field not be orthogonal to the conductor. Figure 3-1 shows a diagram of the waveguide, the electric field,  $E$ , the magnetic field,  $B$ , and the direction of propagation,  $Z$ , of an electromagnetic wave which would be supported by the waveguide. The magnetic field lies parallel to the width of the waveguide, the "a" dimension. The electrical field lies parallel to the height of the waveguide, the "b" dimension. The magnetron probe produces a vertically polarized electric field and satisfies the boundary conditions of a waveguide. The dominant mode supported by a waveguide is the  $TE_{10}$  mode. The

Figure 3-1: Standard waveguide notation. The electric field,  $E$ , the magnetic field,  $B$ , and direction of propagation,  $Z$ .



**S = Conductor Surface**



notation  $Tx_{m,n}$  is used to characterize the different modes supported in a waveguide.  $x$  is either E or M and refers either to the electric or magnetic field;  $m$  refers to the number of half-wavelengths which will fit along the magnetic field axis (the "a" dimension), and  $n$  refers to the number of half-wavelengths which will fit along the electric field axis (the "b" dimension). Figure 3-2 shows the electric and magnetic field distributions inside a waveguide. The electric field is at a maximum at  $\lambda/4$  from the end of the waveguide, while the magnetic field is at a maximum at  $\lambda/2$  from the end of the waveguide.

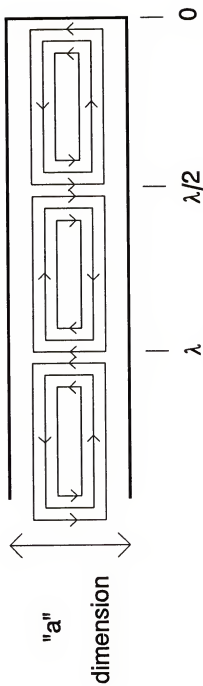
The role of the waveguide is to support the standing microwave field which is formed as the electromagnetic wave emitted from the magnetron is reflected from the front and back walls of the waveguide. In order for this to occur, the magnetron must be inserted a distance of  $\lambda/4$  from the end of the waveguide. The electromagnetic wave emitted by the magnetron travels  $\lambda/4$  to the wall of the waveguide, undergoing a  $90^\circ$  phase shift, reflects off the wall, undergoing a  $180^\circ$  phase shift, and travels back toward the magnetron, undergoing a  $90^\circ$  phase shift. Since the total phase change is  $360^\circ$ , the reflected wave constructively interferes with the outgoing wave and no energy is lost. The electrode is also placed a distance of  $\lambda/4$  from the other end of the waveguide. Here the electric field is at a maximum, and the coupling of the electrode to the field is most efficient. Other factors which determine the extent of coupling include, the degree of penetration of the electrode into the field, and the length of the electrode.

The propagation of a wave in a waveguide depends upon the frequency of the wave. The angle of incidence that the plane wave makes with the waveguide wall

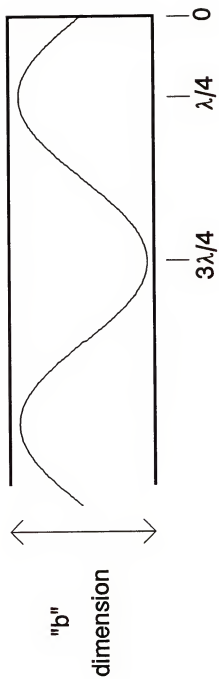
Figure 3-2: The magnetic and electric field distribution inside a waveguide. 0 represents one fixed wall along the length of the waveguide.



# Magnetic Field Distribution



# Electric Field Distribution



becomes greater as the wavelength becomes longer. When the angle of incidence reaches  $90^\circ$ , the wave is completely attenuated. The longest wavelength which will be supported by a waveguide in the dominant  $TE_{10}$  mode is equal to twice the width of the waveguide, and is known as the cutoff wavelength,  $\lambda_c$ . The waveguide must be wide enough to support the operating wavelength of the magnetron.

Due to the finite impedance associated with the waveguide, the actual wavelength in the waveguide,  $\lambda_g$ , is greater than the free-space wavelength,  $\lambda_0$ . For an air filled waveguide, this can be calculated using the equation below:

$$\lambda_g = \frac{\lambda_0}{\sqrt{1 - \left(\frac{\nu_c}{\nu}\right)^2}}$$

where  $\lambda_0$  is the free space wavelength,  $\nu_c$  is the cutoff frequency of the waveguide, and  $\nu$  is the operating frequency of the magnetron.<sup>118</sup>

#### Instrumentation Used in This Work

A capacitively coupled microwave plasma (CMP) consists of a magnetron which emits microwaves into a waveguide. As described previously, the waveguide is of the proper dimensions to support a standing microwave. These microwaves are capacitively coupled to an electrode, which sits at the other end of the waveguide. The electrode is supported in a modified ICP quartz torch, where the central channel of the torch has been widened to accommodate an electrode. Solutions are typically nebulized through a 1 mm

hole which has been drilled through the electrode, and into a plasma which is supported on the tip of the electrode.

Nebulization; however, cannot be used with viscous samples or when the sample size is small. Therefore, a method of discrete sample introduction had to be devised. Ali and Winefordner<sup>119</sup> performed work using a tungsten filament electrode, which not only was used to support the plasma, but also to hold the sample. This resulted in the complete transfer of the sample into the plasma. This work is based upon that of Ali and Winefordner,<sup>119</sup> who characterized the tungsten filament electrode for the discrete sampling of aqueous solutions into a CMP.

The electrode was similar to that used by Ali and Winefordner;<sup>119</sup> however, some modifications were made to improve its performance. Their electrode was formed by making a loop in the tungsten wire by twisting the wire over itself. The ends of the wire were bent to be perpendicular to the loop. Shoulders were added to the ends of the wire by kinking the wire. These shoulders were used to keep the electrode from falling into the central channel of the modified ICP torch. The plasma formed not only on the loop of the wire, but on the shoulders as well, decreasing the amount of power that was available for atomization of the analyte. This work uses the same 0.25 mm diameter tungsten wire to form the electrode. However, the wire was tied in a knot to form the loop. The ends of the wire were then bent perpendicular to the loop, and the wire was held in the central channel of the torch by compression of the wire against the torch walls. This resulted in no sharp discontinuities in the electrode where a plasma could

form. Instead, the plasma formed only at the top of the loop where the analyte was located.

Microliter volumes of sample were deposited on the loop of the electrode. The sample was dried at low microwave powers ( $<70$  W). The microwaves resistively heated the wire, and also interacted directly with the sample. The power was decreased and the plasma gas was initiated. Helium was used as the plasma gas due to its great excitation efficiency and low background. After, the helium was added the power was increased which resulted in the autoignition of the plasma, and the atomization and excitation of lead. A monochromator and photodiode array was used to detect the transient emission.

The CMP spectrometer is shown in Figure 3-3. The components are described in Table 3-1. The magnetron output power is directly related to the power input from the high voltage dc power supply, which negatively biases the cathode of the magnetron. Two dc power supplies were used. At first only a voltage-regulated supply was available (the Hipotronics power supply, model 803-330), and was regulated only within 15 %. This power supply was specified to provide only 3000 V, although at full scale it produced closer to 4000 V. Since work was always performed above 3000 V and the voltmeter on the power supply did not go above 3000 V, a voltage divider was put in parallel with the magnetron to allow safe measurement of the voltage output by the power supply. The current through the magnetron was measured by placing a  $1\ \Omega$  resistor in series with the magnetron. The Hipotronics power supply was used for some of the

Figure 3-3: The capacitively coupled microwave plasma atomic emission spectrometer.

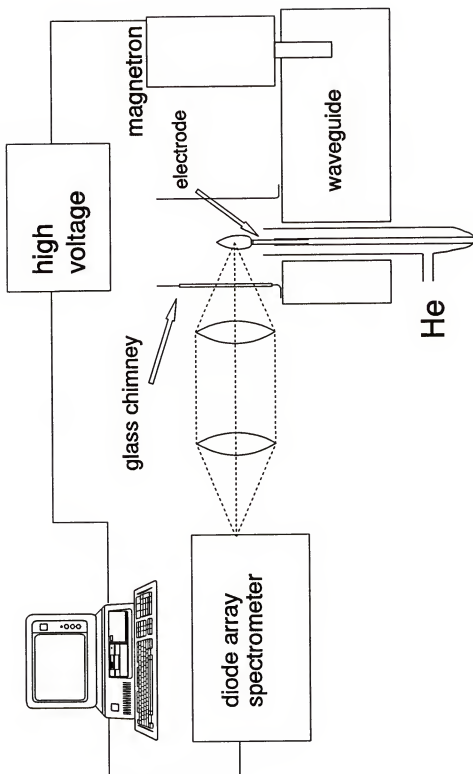


Table 3-1 CMP Instrumentation

Apparatus / Manufacturer/ Description	Model	Location of Manufacturer or Supplier
D.C. Power Supply		
Hipotronics 3000 V at 330 mA	803-330	Hipotronics, Inc Brewster, NY
Bertran 5000 V at 200 mA	106-05R	Bertran High Voltage Hicksville, NY
A.C. Power Transformer		
Magnetek Triad 6.3 V at 25 A	F-28U	Newark Electronics Chicago, IL
High Voltage Reed Relay		
Magnecraft	W102VX-49	Newark Electronics Chicago, IL
Magnetron		
Samsung 870 W	OM-75A	Richardson Electronics Lafox, IL
Aluminum Waveguide		
Lab constructed (LxWxH) 280 mm x 90 mm x 46 mm		
Quartz Plasma Torch		
Lab constructed 2-tube concentric (16 mm o.d., 3 mm i.d.)		

Table 3-1--Continued

Apparatus / Manufacturer/ Description	Model	Location of Manufacturer or Supplier
Computer		
PC's Limited 8 MHz - 286	28608L	PC's Limited Austin, TX
D/A and A/D converter		
SRS Computer Interface	SR 245	Stanford Research Systems Palo Alto, CA
Boxcar Averager		
SRS Gated Integrator and Boxcar Averager	SR 250	Stanford Research Systems Palo Alto, CA
Photomultiplier Tube		
Photomultiplier Tube	1P28	Hammamatsu Corporation Bridgewater, NJ
Photomultiplier Power Supply		
Pacific High Voltage Power Supply	226	Pacific Precision Instruments Concord, CA
Monochromator		
Spex 0.5 m Monochromator 1200 grooves/mm 300-nm blaze wavelength	1870	Spex Edison, NJ
Intensified Photodiode Array		
Tracor Northern	TN-6122A	Tracor-Northern Middleton, WI
Photodiode Array Controller		
Tracor Northern	TN-6500	Tracor-Northern Middleton, WI



aqueous work. A current-regulated high voltage power supply (Bertran, model 105-06R) was later obtained when funds became available. This power supply greatly improved the precision of this work, and provided up to 5000 V at 200 mA. The power supply was operated in the current regulated mode, and was also analog programmable, so that, in conjunction with a digital to analog converter, it could be operated under computer control. This power supply was used for all the analyses of lead in whole blood. A computer program written in QuickBasic® was used along with the Stanford computer interface listed in Table 3-1, to control the output of this power supply.

The dc high voltage was connected to the secondary of a low voltage ac transformer. The ac transformer was connected to the tungsten wire in the magnetron cathode, and resistively heated the tungsten wire producing the thermionic emission necessary for operation of the magnetron. The ac transformer was on continuously. A general wiring diagram for the microwave power supply and further information can be found in references by Meiners and Alford,<sup>120</sup> and Chilukuri and Lichten.<sup>121</sup>

A monochromator and photodiode array were used to detect the transient emission signal resulting from the atomization step in the plasma. The light from the plasma was collimated, and refocused into the monochromator, using standard 1:1 imaging. The monochromator had a focal length of 0.5 m. The monochromator was typically used with a slit width of 120  $\mu\text{m}$ , and provided a resolution of approximately 0.2 nm.

The detector consisted of an intensified 1024 element diode array. The diode array consisted of a linear array of silicon photodiodes each of which were equally spaced by 25.4  $\mu\text{m}$ . The peak sensitivity of the photodiodes fell at 750 nm. The

intensifier shifted the peak sensitivity to between 450 and 550 nm, and provided a maximum gain of 6,000 over the equivalent non-intensified photodiode array. The peak quantum efficiency of this detector was approximately 12 %.

The diode array operated in a charge-storage mode. Incident radiation on the detector is converted to a charge. After a specified integration time, the charge on each diode is determined sequentially, and the diodes are discharged. The integration time is specified by the user, and is limited by the readout time of the array. The readout time is 10  $\mu$ s per diode plus a 300  $\mu$ s overhead. It took approximately 10 ms to readout the array. Since the entire array must be read out after every integration period, too short an integration time lowered the duty cycle of a measurement. Further information on diode array operation can be found in a reference by Ingle and Crouch.<sup>122</sup>

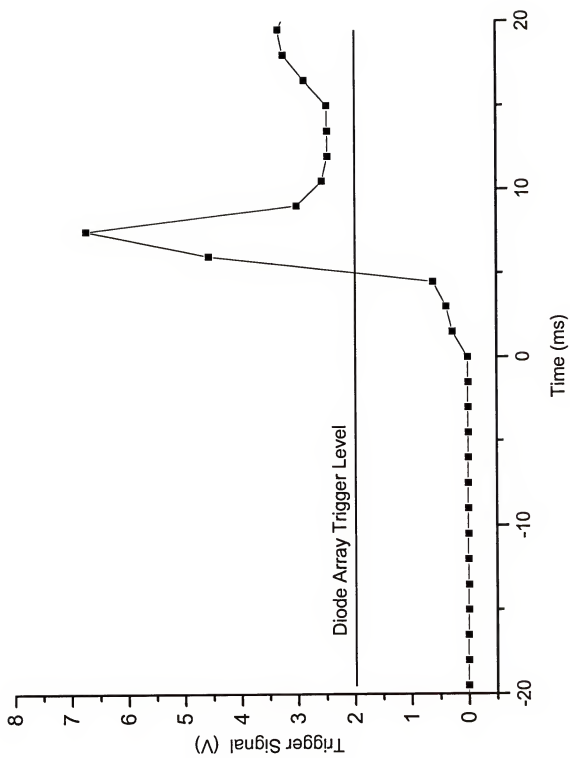
The monochromator dispersed a 40 nm wavelength region across the array. Simultaneous background correction is possible, which is particularly advantageous in emission spectroscopy where the background is known to vary in time. In addition, spectral interferences can be identified easily with a photodiode array. A disadvantage of the diode array is its cost.

The diode array was triggered to start collecting data in one of two ways, depending on whether an aqueous or whole blood sample was analyzed. With aqueous samples, the detector was triggered off the light that emanated from the plasma. After the aqueous sample had been dried, the helium gas flow initiated, and the microwave power increased to form a plasma, the light from the plasma was used to trigger the photodiode array. The light from the plasma was detected with a photomultiplier tube

(PMT) which was protected from overexposure using a neutral density filter. The PMT current was converted to a voltage using a transimpedance amplifier, and sent into the input of an operational amplifier (op-amp). The operational amplifier was used as a voltage follower with gain.<sup>123</sup> Since only 12 V was supplied to the op-amp, it soon became saturated at a level well below that which would harm the trigger input on the photodiode array. This circuit had a response time of less than 6 ms, and was useful in synchronizing the plasma ignition with the detection electronics. The trigger signal is shown in Figure 3-4. This was the first attempt in our laboratory to synchronize the plasma ignition with the detection electronics. Ali *et al.*<sup>124</sup> first triggered the photodiode array, and then ignited the plasma. Afterwards, they sorted through the spectra collected to determine when the plasma ignited. This is an inefficient process, especially when the number of spectra collected is great.

With the blood samples, a plasma ashing stage was used after the drying stage. After drying the blood sample, a low power plasma was used to ash the sample before a higher power plasma was used to atomize the sample. Since the plasma was never turned off a light-based trigger was not useful. In this case, the digital to analog converter controlling the dc power supply was used to send a TTL HI (>2.4 V) signal to the diode array trigger input just before the power was increased. This triggering method was not used in the case of aqueous samples, since there was a variable delay between the increase in power output of the supply and the ignition of the plasma.

Figure 3-4: The output of the triggering circuit versus time. 0 ms corresponds to the ignition of the plasma.



### Determination of the Optimum Length and Position of the Electrode

The coupling of the electrode to the electric field is known to depend on the length of the electrode, the position of the electrode within the electric field, as well as the distance of the electrode from the waveguide wall. The distance of the electrode from the waveguide wall was fixed at  $\lambda/4$ . The remaining parameters to be optimized included the length of the electrode, and the depth of penetration of the electrode into the electric field (i.e. the vertical position of the electrode with respect to the waveguide).

### Experimental

The extent of coupling of the electrode to the electric field was determined by moving the electrode vertically relative to the waveguide every 3 mm, and then measuring the minimum power necessary for the plasma to be sustained. The power was increased by operating the power supply in the current-regulated mode, and increasing the current incrementally by 2 mA from a base current of 15 mA until a plasma could be sustained. A metal wire was used to ignite the discharge by touching the wire to the electrode. If the plasma did not extinguish after the wire was removed, then the power, voltage, and current were recorded. Better coupling was achieved at a position where the plasma can be sustained at a lower power. This experiment was carried out using electrodes of different lengths: 65 mm, 60 mm, 55 mm, 50 mm, 45 mm, and 40 mm.

### Results

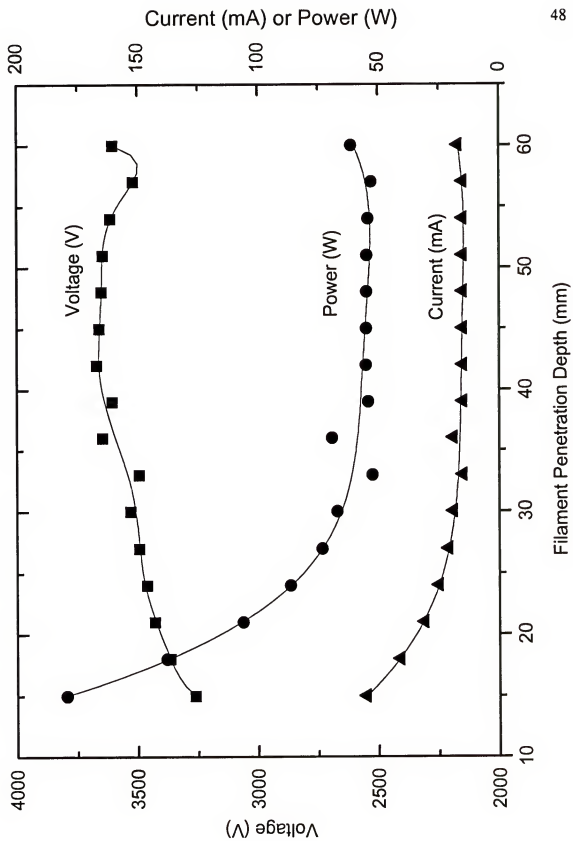
The 40 mm and 45 mm electrodes could not be used in analytical determinations since a plasma was just as likely to ignite on the bottom of the electrode, as on the top.

The 50 mm through 65 mm electrodes were all equally useful. A profile of the voltage, power, and current curve is shown for the 65 mm electrode in Figure 3-5. For a small change in current, there was a large change in power, although, there is little dependence of the power on the applied voltage. The optimum coupling of the electrode to the field occurred when the bottom of the electrode penetrated the waveguide by at least 3 cm. This corresponded to approximately  $1/4$  the waveguide wavelength,  $\lambda_g$ . The electrode used to support the plasma acts much like a "cavity antenna"<sup>125</sup> which is used to transmit energy out of a waveguide, the optimum position for coupling for a cavity antenna is  $1/4 \lambda_g$ .

One unique feature of the CMP versus the MIP and ICP is that it autoignites at fairly low applied voltages. This can be attributed to the small diameter of the electrode upon which large electric field strengths are generated. A spark is not necessary to ignite the plasma, as in an MIP or ICP. As seen in Figure 3-5 if the electrode penetrated the waveguide by more than 3 cm, the voltage increased for a given current. Since it is necessary to exceed the breakdown potential of the gas in order for the plasma to autoignite, the tungsten electrode was placed 3.5 cm into the waveguide. Approximately 3600 V, as measured on the dc power supply was necessary to breakdown the helium gas. This autoignition feature is especially important for discrete sampling in the CMP, where it is necessary to create a stable plasma rapidly, before the analyte is vaporized off the electrode.

Figure 3-5: The minimum power required for a plasma to be sustained versus the depth of the electrode in the waveguide.





### Conclusions

Magnetrons are used to generate energy at microwave frequencies. They are coupled to a waveguide which transfers energy to the electrode much more efficiently than conventional transmission lines, i.e. coaxial cable. Such a device is very inexpensive. The optimum coupling of the electrode to the waveguide was determined to be independent of the length of the electrode, but depends on the insertion depth of the electrode into the waveguide. When the bottom of the electrode penetrated the cavity by  $> 3.0$  cm, coupling was optimum and the plasma would autoignite.

## CHAPTER 4 THE DETERMINATION OF LEAD IN AQUEOUS SAMPLES USING DSI-CMP-AES

### General Introduction

Ali and Winefordner<sup>119</sup> first characterized the use of a tungsten filament electrode for the discrete introduction of aqueous samples into a capacitively coupled helium/hydrogen microwave plasma. Excellent absolute detection limits in the 1 - 100 pg range were obtained for 12 elements using 2  $\mu$ L aliquots. The precision ranged from 5 to 10%. However, Pb was not one of the 12 elements studied. Therefore, it was of importance to characterize the use of this discrete sample introduction technique for the determination of lead. In this chapter, several aspects of a pure He CMP are characterized with the main goal of determining Pb at concentrations below 100 ppb with a precision less than 10 %.

### Selection of Wavelength

#### Introduction

One of the major disadvantages of any electrode supported plasma - i.e. the glow discharge, DC Arc, DCP, or CMP, is the emission that originates as the electrode itself decomposes, and is atomized and excited. Emission from the plasma support gas and small molecular species found in plasmas - i.e. OH, CN, etc. must also be avoided.

Therefore, it is of paramount importance to select an analytical emission line which is well resolved from the emission background due to the electrode, the plasma support gas, and to a lesser extent due to their generally weaker intensity, from molecular species which may be present. In addition, the analytical emission line must be sufficiently sensitive to yield the necessary detection limit. The relative Pb emission intensities observed by Vermaak *et al.*<sup>126</sup> in a 600 W Pt-clad, tungsten electrode supported air-plasma CMP are shown in Table 4-1.

Table 4-1 Relative Emission Intensities in an air-plasma CMP

Wavelength (nm)	Relative Signal	Relative Background	Signal/Background
405.8	100	1.0	100
368.3	65	1.8	36
364.0	30	1.6	19
283.3	43	5.5	8
280.2	22	3.7	6

### Experimental

#### Procedure

Initial work started with a tungsten electrode supported helium plasma similar to that used by Ali and Winefordner.<sup>119</sup> The background spectrum was characterized at each of the wavelengths shown in Table 4-1. The forward power was 170 W. For those wavelengths that looked promising, the lead signal to noise ratio was determined in the following manner: 5  $\mu$ L of a 22 ppm Pb standard was deposited on the electrode with an air displacement pipet, dried capacitively for 90 s at 70 W, and then atomized at

170 W. The He flow rate was 10 L/min, and was initiated after the drying step since, at the power used during the drying step, a He plasma would have ignited. No purge gas is present during the drying step.

### Reagents

All Pb solutions used were prepared by serial dilution of a commercially available 1000 ppm atomic absorption standard (Fisher-Scientific, Pittsburgh, PA).

### Results

Tungsten has a rich spectrum near 280 nm as shown in Figure 4-1. In fact, a tungsten line at 283.3 nm completely prevents the determination of Pb at the same wavelength. The background in this region is also very structured, making the determination of Pb at 280.2 nm very difficult. Background spectra obtained at 364.0, 368.3, and 405.8 nm were much cleaner with no tungsten interferences within 1 nm of the lead emission line; however, a weak molecular background was present in all cases. Figure 4-2 depicts the emission spectra of Pb at both 364.0 nm and 368.3 nm. Both wavelengths are completely free from W emission; however, a weak molecular background is present. The emission spectra of Pb at 405.8 nm is presented in Figure 4-3. Potential interferences in this region include two tungsten emission lines at 404.6 and 407.0 nm, and a molecular background with a bandhead at 405.9 nm which is degraded toward the ultraviolet (This cannot be seen under the Pb peak in Figure 4-3, but will be discussed later in this chapter). Both tungsten lines are over 1 nm away and are therefore easily resolved from the Pb emission line; however, the molecular emission

Figure 4-1: Tungsten emission background around 280 nm. Pb emission would lie at 280.2 nm and 283.3 nm. Monochromator slit width = 120  $\mu\text{m}$ .

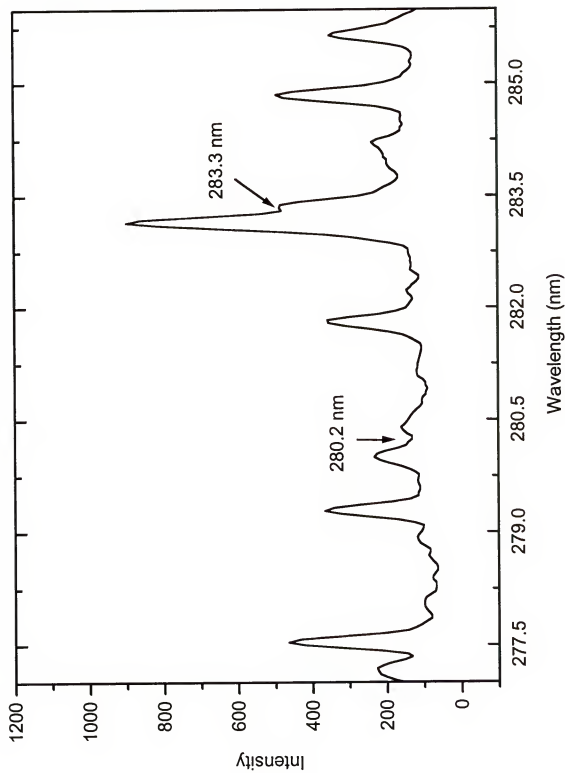


Figure 4-2: Pb emission at 364.0 nm and 368.3 nm. 110 ng of Pb was used. Monochromator slit width = 120  $\mu\text{m}$ .



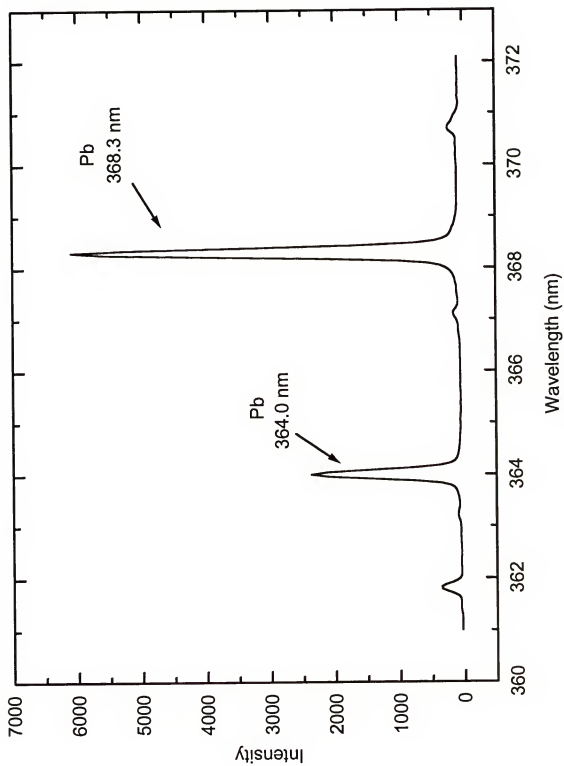
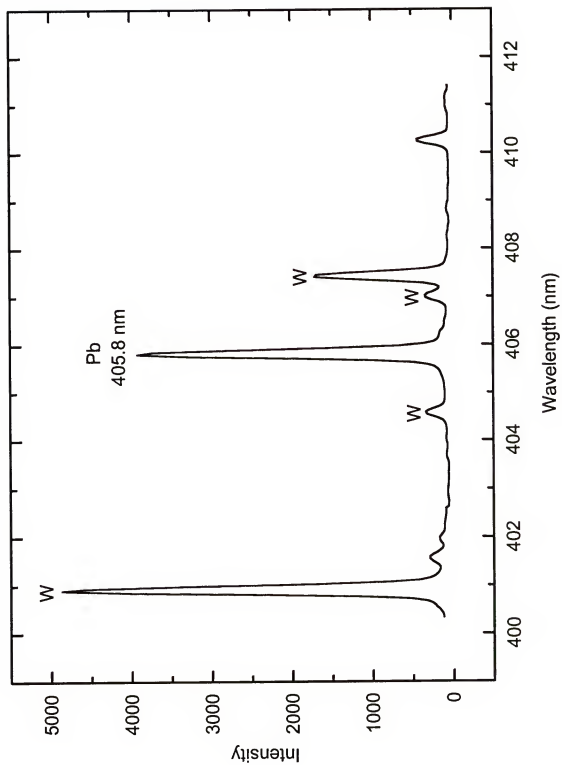


Figure 4-3: Pb emission at 405.8 nm. 110 ng of Pb was used. Monochromator slit width = 120  $\mu\text{m}$ .



cannot be resolved and required that a blank be measured. Since the baseline was not flat, a simple off-wavelength correction scheme would not have been adequate. The signal to noise ratio for lead was determined for these 3 wavelengths and the results are shown in Table 4-2. The larger signal for the line at 368.3 nm compared to the line at 405.8 nm is an artifact of the detection system. When corrected for the response of the spectrometer the intensity of the 405.8 nm line is actually 1.22 x greater than the 368.3 nm line. In any case, the signal to noise ratio is greatest at 405.8 nm and was used in subsequent work.

Table 4-2 Pb Signal/Noise Ratio at 364.0, 368.3 and 405.8 nm

Wavelength (nm)	Signal	Noise	Signal/Noise
405.8	14532 $\pm$ 894	16.9 $\pm$ 2.7	874 $\pm$ 105
368.3	22169 $\pm$ 2183	29.7 $\pm$ 3.2	752 $\pm$ 83
364.0	7894 $\pm$ 964	13.0 $\pm$ 2.8	618 $\pm$ 74

### Selection of Electrode Material

#### Introduction

The tungsten emission intensity was observed to increase as the electrode aged. This resulted in a decreased signal to noise ratio for Pb. Therefore, other possible electrode materials were examined. No comparative study had been performed on the range of materials which might be used in a wire-electrode based CMP. Tungsten had initially been chosen since it has the highest melting point (3683 K) of all metals. However, tungsten is hardly ideal as it is very reactive, forms an oxide readily, and has

a fairly rich spectrum. In addition, if different metal electrodes could be used, then one could simply switch to a different metal electrode if a spectral interference occurred. The electrode must have a higher melting point than the plasma gas temperature and must be conductive.

### Experimental

#### Electrodes

The wires necessary to make the electrodes were obtained from AESAR / Johnson Matthey, Ward Hill, MA.

#### Procedure

The background emission spectra of the materials shown in Table 4-3 were characterized at 405.8 nm. A He discharge was ignited for a period of 10 seconds at a power of 170 W on each electrode. Some of the electrodes melted. Each electrode material was fired three times to ensure that the results obtained were consistent.

#### Results

Most of the electrodes melted before the 10 s period had expired. More precisely, the tip of the electrode which was in direct contact with the plasma melted. However, the tungsten, molybdenum, and Pt-clad tungsten electrodes survived. The Pt-clad tungsten electrode; however, lost its Pt-coating as soon as the discharge had ignited limiting its usefulness. It is surprising that the Mo electrode survived while the Ta electrode did not, since pure Ta has a higher melting point than pure Mo. Perhaps the lower purity level of the Ta electrode depressed its melting point to lower than Mo.

Table 4-3 Different Electrode Materials

Element	Diameter (mm)	Melting Point (°C)	Metal Purity (%)
W	0.25	3410	99.98
V	0.127	1890	99.8
Pt	0.25	1772	99.998
Mo	0.25	2617	99.97
Ni	0.25	1453	99.994
Ti	0.25	1660	99.99
Ta	0.25	2996	99.9
Pt-Clad W	4 $\mu$ m on 0.25	-	-

Also, the thermal conductivity of Ta, which is only 0.4 times that of Mo was insufficient to dissipate the heat along the length of the electrode before it melted.

This experiment implies that the gas temperature of the plasma at a power of 170 W lies between the melting points of V and Mo, 2163 K and 2830 K. This agrees with the spectroscopic temperature measurement of Ali and Winefordner,<sup>127</sup> who found that at a power of 100 W, the temperature of the tungsten filament He-CMP was approximately 2400 K.

The tungsten and molybdenum emission spectra are shown in Figure 4-4. Molybdenum emission lines nearest the Pb emission at 405.8 nm appear at 406.2 nm and 407.0 nm. Because molybdenum requires greater resolution than tungsten to be separated from the lead emission, tungsten was determined to be the electrode of choice.

### Evaluation of the He Purge Time

#### Introduction

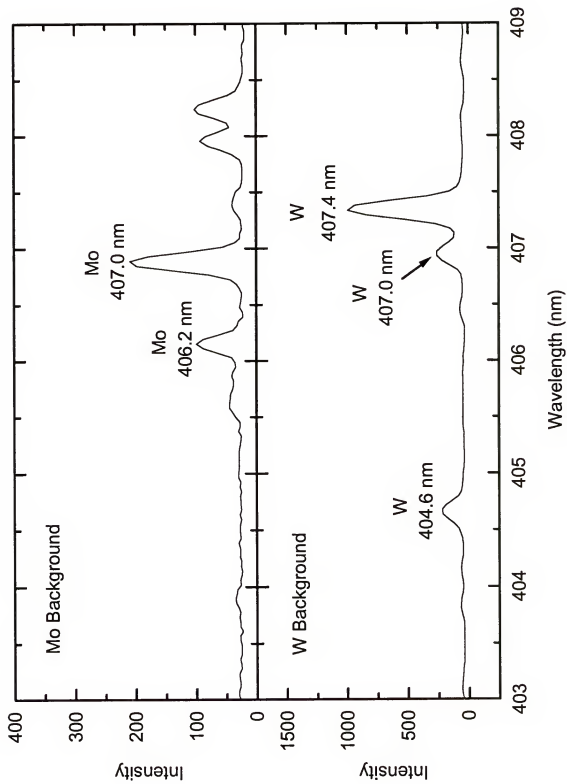
Some molecular emission was observed in the 405.8 nm wavelength region which had a bandhead at 405.9 nm. An experiment was performed to identify if the source of this emission originated from the electrode, from air entrainment into the atmospheric pressure plasma, or from impurities in the He plasma gas.

#### Experimental

Helium at a flow rate of 10 L/min was allowed to purge the torch for increasing amounts of time prior to igniting the plasma. The emission was measured when the plasma ignited. If air entrainment into the plasma was the source of the molecular

Figure 4-4: (TOP) Mo emission background around 405 nm.  
(BOTTOM) W emission background around 405 nm.





emission, then longer purging times should have resulted in a lower molecular emission background.

## Results

The results are shown in Figures 4-5 to Figure 4-7. The diode array was triggered when the plasma ignited, and was read out every 0.18 s. Five spectra are shown in each plot which represent the time periods from 0.18 to 0.90 s. This corresponds to the time interval when lead emission is observed. Figure 4-5 to Figure 4-7 depict the results of 5, 30, and 300 s helium purges, respectively, prior to igniting the plasma. In Figure 4-5, emission resulting from  $N_2^+$  was observed at 405.9 nm, and the tungsten background was very intense. The molecular peak at 405.9 nm was identified using a standard wavelength table,<sup>128</sup> was observed in a pure  $N_2$  plasma, and also when compressed air at a flow rate of 100 mL/min was added to the He plasma. In Figure 4-6, the baseline between the tungsten peaks is very flat and the tungsten emission has been greatly reduced. In Figure 4-7, only a high fixed frequency noise was observed. Fixed frequency noise has been observed previously on diode array spectra and is attributed to the feedthrough of the clocking signals, and occurs at exactly 1/4 of the clock frequency.<sup>129</sup> This noise was only observed when the emission background was low (<100 counts). The frequency of the noise was identified as 0.032/diode by taking the Fourier transform of the noise, and subsequently a filter was created which blocked only this frequency. The application of this filter to lead signals is discussed later in this chapter. These results show that the source of molecular emission was due

Figure 4-5: Results of a 5 s helium purge. Monochromator slit width = 120  $\mu\text{m}$ .

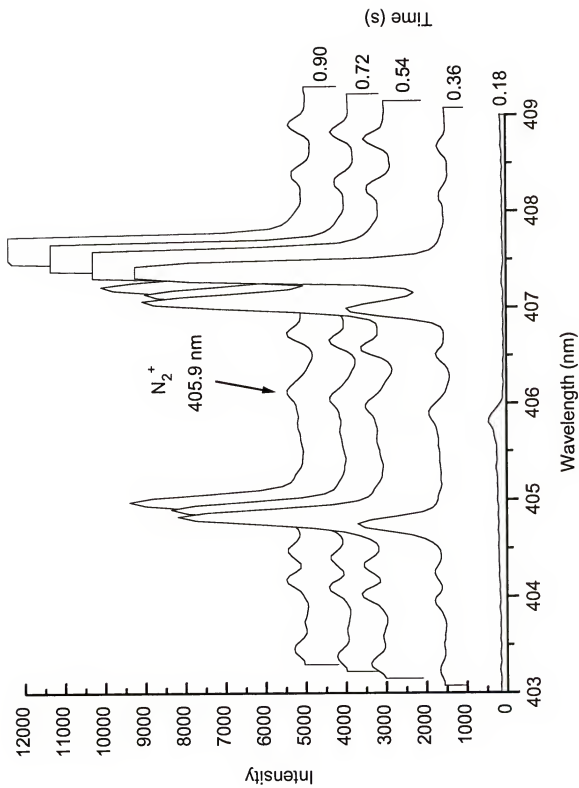


Figure 4-6: Results of a 30 s helium purge. Monochromator slit width = 120  $\mu\text{m}$ .

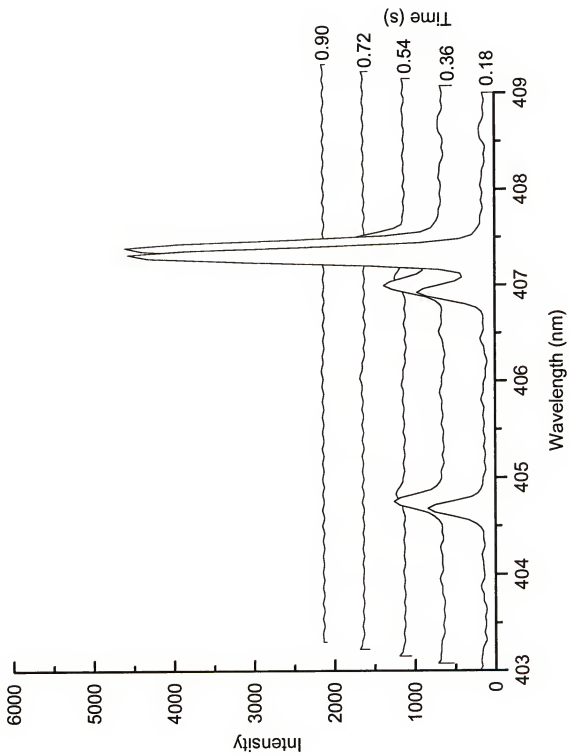
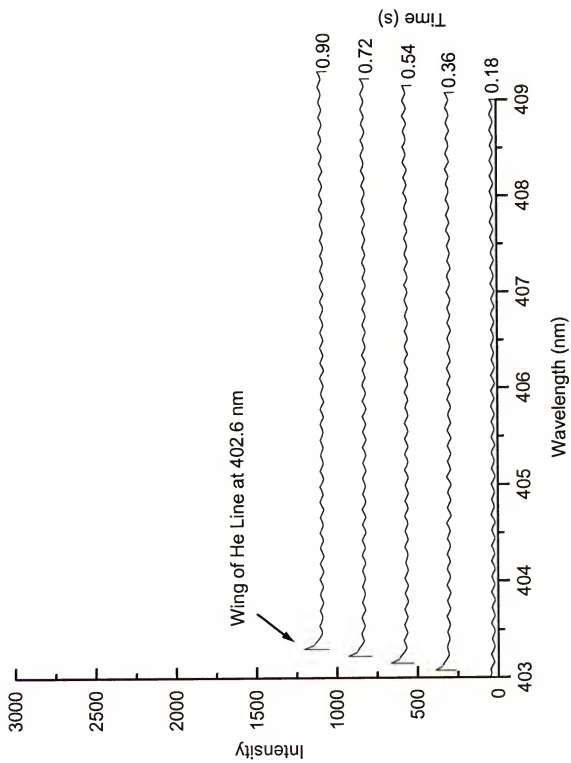


Figure 4-7: Results of a 300 s helium purge. Monochromator slit with = 120  $\mu\text{m}$ .





to air entrainment into the plasma and therefore, a smaller, lower dead volume torch which could be purged with a lower He flow rate and in a shorter time should be beneficial. In addition, since it was possible to remove all the background tungsten emission, determination of an element which had an emission line which coincided with a tungsten emission line would be possible. Apparently, W must be oxidized before W emission is seen, i.e. the volatility of W is low at approximately 2400 K. Concerning the determination of lead, the signal to noise ratio improved up to a purge time of 30 s, but did not improve thereafter. Apparently, 30 s was enough to reduce the mole fraction of  $N_2$  to levels where the  $N_2^+$  emission was below the detection limit of the instrument. In addition, the purge lengthened the life of the electrode.

### Flow Rate Optimization

#### Introduction

Helium is the most expensive of the gases typically used in plasmas, i.e.  $N_2$  and Ar. Helium is approximately twice as costly as Ar and ten times as costly as  $N_2$ . Therefore, it was important to determine the minimum He flow rate that yields the best signal to noise ratio for Pb.

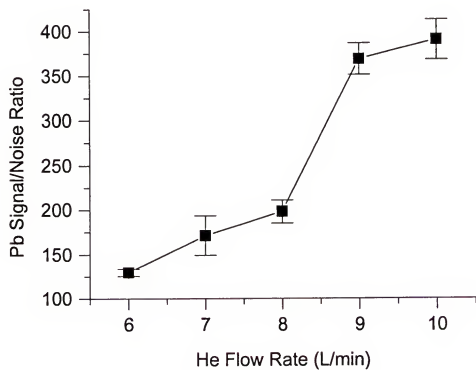
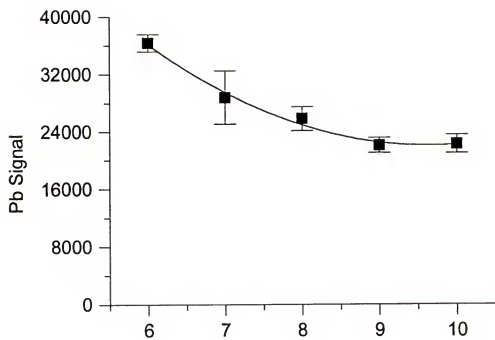
#### Experimental

Five  $\mu\text{L}$  aliquots of a 1 ppm Pb standard were deposited on the electrode, dried at 70 W, and then atomized at 170 W.

#### Results

The results obtained are shown in Figure 4-8. The Pb signal decreased with an increase in the He flow rate; however, the noise increased rapidly. The increase in noise

Figure 4-8: Lead signal and signal/noise ratio versus the helium flow rate. The error bars represent 1 standard deviation based on 6 measurements.



is mostly a result of increased air entrainment which oxidized the electrode resulting in greater tungsten emission and the increased  $N_2^+$  emission at 405.9 nm. A higher flow rate; however, decreased the residence time of the Pb in the plasma, and resulted in greater cooling of the plasma, perhaps decreasing the atomization efficiency. The best results were obtained at a He flow rate of 10 L/min. Higher flow rates were not tested due to the high cost of He.

### Radial and Axial Profile

#### Introduction

The spatial distribution of Pb emission in the plasma was briefly characterized. The whole plasma was not imaged into the spectrometer; therefore, it was important to determine the spatial variation of the Pb signal to noise ratio. In addition, such a study revealed the critical alignment process when a new electrode had to be inserted.

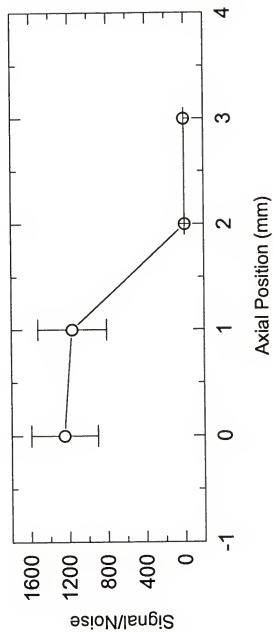
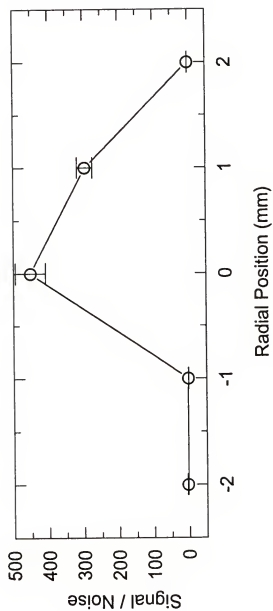
#### Experimental

The radial optimization was performed using 5  $\mu$ L of a 64 ppb Pb standard (320 pg Pb). The axial profile was performed using 5  $\mu$ L of a 2 ppm Pb standard. The samples were dried for 90 s at 70 W, and atomized at 170 W.

#### Results

Figure 4-9 shows both the radial and axial profiles. The lead signal to noise ratio is optimum within 1 mm of the top of the electrode. In addition, the lead signal to noise ratio is optimum within 1 mm of the center of the plasma. The alignment process is

Figure 4-9: (TOP) Radial Pb emission profile. 320 pg of Pb was used. Error bars represent 1 standard deviation based upon 3 measurements. Position 0 represents the center of the plasma.  
(BOTTOM) Axial Pb emission profile. 20 ng of Pb was used. Error bars represent 1 standard deviation based upon 3 measurements. Position 0 represents the top of the electrode.



critical to the performance of the device, and one must be within 1 mm of the optimum in both the axial and radial directions to have a maximum signal to noise ratio.

### Power Optimization

#### Introduction

The power applied to the plasma is known to influence both the atomization and excitation efficiency of an analyte. For these reasons, the Pb signal to noise ratio was monitored as a function of the applied power.

#### Experimental

Two  $\mu\text{L}$  of a 10 ppm Pb standard was used. The sample was dried using the same conditions as in previous studies, followed by atomization at higher powers.

#### Results

The lead signal was integrated over a period of 3 s from ignition of the plasma. Representative temporal profiles are shown in Figure 4-10. The signal profile becomes sharper and more intense as the power is increased. However, above 172 W there is no gain in the integrated signal to noise ratio, Figure 4-11. At 172 W, the electrode could sustain approximately 200 firings, while at powers greater than 250 W, the electrode lasted only 5 firings. Therefore, a power of approximately 170 W was used in further studies. At a power of 170 W, the FWHM of the temporal emission profile was approximately 0.11 s.

### Calibration Curve

Several calibration curves were measured following each optimization in order to determine the figures of merit for Pb.

Figure 4-10: Pb emission signal vs time at different powers. Two microliters of 10 ppm Pb was used.



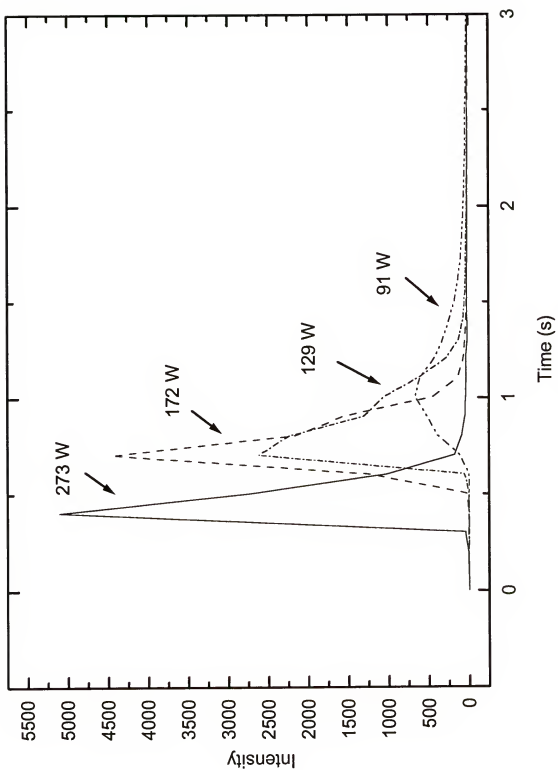
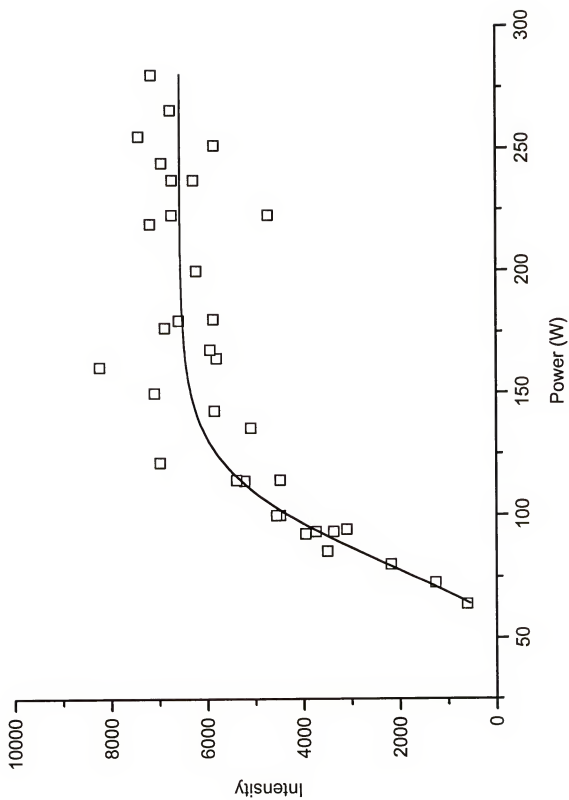


Figure 4-11: Pb emission signal versus power. Integration time = 3 s.



### Experimental

Lead solutions were prepared by serial dilution of a commercially available 1000 ppm aqueous Pb standard. Aqueous samples of 10  $\mu\text{L}$  volume were deposited on the electrode with an air displacement pipet and dried at 75 W for 90 s. After the drying step, the microwave power was decreased to 13 W and the helium plasma gas flow rate was set to 10 L/min. The microwave power was then increased to 170 W which ignited the plasma and atomized and excited the sample. A photodiode array spectrometer detected the transient lead emission signal. The photodiode array was triggered to start acquiring data when the plasma ignited, and was read out every 0.18 s for forty successive times resulting in a time resolved profile of the lead signal. The results were stored and analyzed with a computer. For all measurements a monochromator slit width of 120  $\mu\text{m}$  was employed.

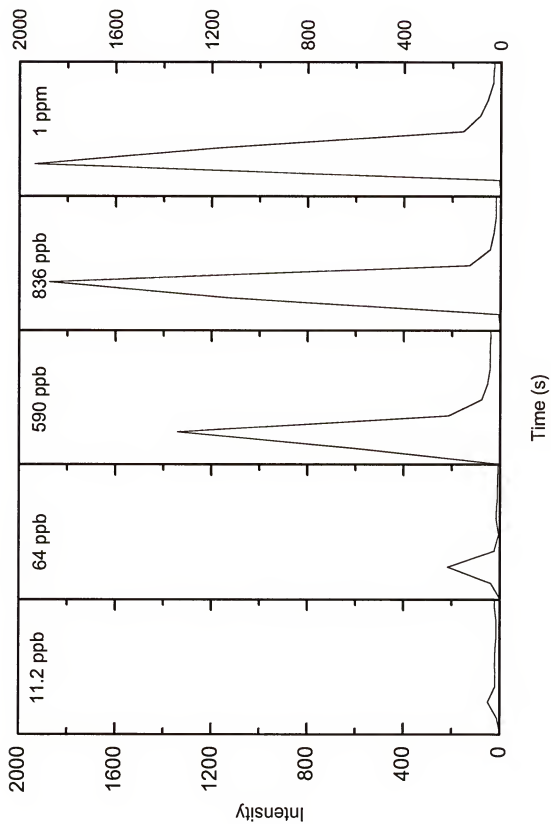
### Results

The results obtained are shown in Table 4-4. Representative temporal profiles are shown in Figure 4-12. The time axis ranges from 0 s to 1.5 s for each temporal profile shown in Figure 4-12. The calibration curve was linear ( $R^2=0.994$ ) from the detection limit to 1 ppm. Previous calibration curves have shown that the Pb emission signal became nonlinear at Pb concentrations greater than 1 ppm. This corresponds to a linear dynamic range of about three orders of magnitude. The concentration detection limit corresponding to three times the noise on the blank was 2 ppb, and the mass detection limit was 20 pg.

Table 4-4 Calibration Curve Results

Concentration (ppb)	Signal	Standard Deviation	% RSD
1000	3809	327	8.59
836	3327	181	5.44
203	2033	200	9.86
64	263	16	6.0
11.2	33	5.8	17

Figure 4-12: Temporal emission profiles of lead at low concentrations. The time axis for each profile is 1.5 s long.



Previous calibration curves have shown that a detection limit of 0.6 ppb (3 pg) can be obtained with 5  $\mu$ L samples. In addition, the % RSD was better than 10 % at concentrations greater than 100 ppb. These limits meet those required by the CDC for a screening device. The concentration detection limit is better than that achieved by nebulization-based AES (see Table 4-5), and the mass detection limit is comparable to that achieved by ETA-AAS (11 pg)<sup>130</sup> and ETV-AES and DSI-AES (again, see Table 4-5). Figure 4-13 depicts a 64 ppb Pb signal and shows the high sensitivity that can be obtained with this device. In addition, it shows the performance of a blocking filter to remove noise without distorting the signal. The difference in the peak height measurement of the Pb signal before and after filtering was < 2%. The total analysis time per sample was less than 2 minutes. No memory effects were observed even at high lead concentrations (> 100 ppm) as long as the plasma was left on for a period of ten seconds.

### Conclusions

The tungsten filament based He CMP is a very sensitive emission technique which can compete with graphite furnace atomic absorption spectroscopy. This results mainly from the high sampling efficiency in which 100% of the sample is introduced into the plasma in a short period of time (0.11 s FWHM). The filament and purge time optimizations dealt with removing a molecular interferent, and reducing the rate of erosion of the electrode. Both were achieved by allowing He to purge the plasma torch for a period of 30 s prior to igniting the plasma. Redesign of the plasma torch to reduce the dead volume of the torch is warranted. In addition, selective determination of an



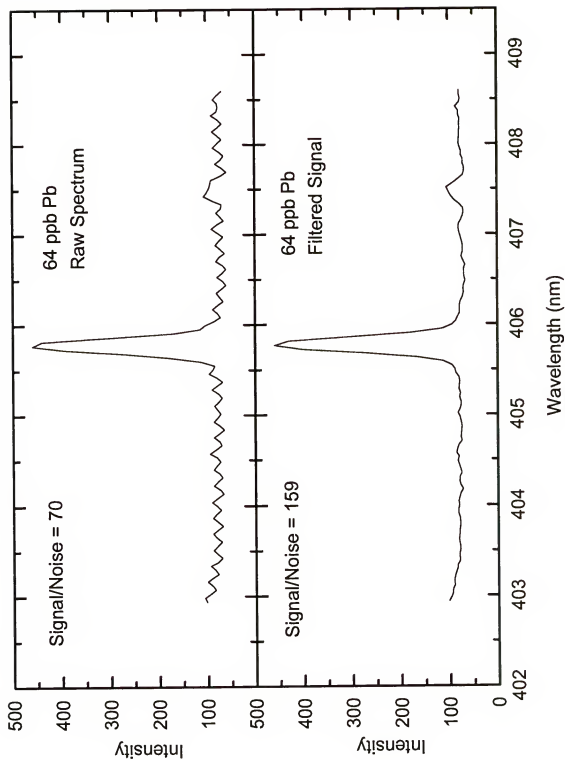
element which overlaps a tungsten emission line is possible with a good He purge. For the determination of Pb, linearity ranged from the detection limit (2 ppb) to 1 ppm. The precision (% RSD) varied from 5 to 10 % at concentrations greater than 64 ppb. The total analysis time per sample was less than 2 minutes. The majority of that time, 90 s is devoted to drying the sample. Further improvements could certainly be made, and are described in Chapter 6.

Table 4-5 Aqueous Pb Detection Limits by Atomic Emission

Plasma	Total Gas Flow Rate	Sample Introduction Method	Wavelength (nm)	Concentration Detection Limit (ppb)	Mass Detection Limit (pg)
300 W Air-MIP <sup>131</sup>	5.8 L/min Air	Pneumatic Nebulizer	368.3	590	-
1.6 kW He-MIP <sup>132</sup>	23 L/min He	Ultrasonic Nebulizer	220.4	700	-
500 W Ar-MIP <sup>133</sup>	3.5 L/min Ar	Pneumatic Nebulizer	405.8	54	-
325 W Ar/N <sub>2</sub> -CMP <sup>134</sup>	0.6 L/min Ar 6.5 L/min N <sub>2</sub>	Pneumatic Nebulizer	405.8	3000	-
500 W Air-CMP <sup>135</sup>	8.5 L/min Ar	Pneumatic Nebulizer	405.8	7600	-
1.3 kW Ar-ICP <sup>130</sup>	14 L/min Ar	Pneumatic Nebulizer	220.4	20	-
1.2 kW Ar-ICP <sup>136</sup>	11 L/min Ar	DSI	220.4	2.1	21
1 kW Ar-ICP <sup>137</sup>	Not Reported	ETV	220.4	7	70
135 W He-MIP <sup>138</sup>	0.4 L/min He	ETV	405.8	1	50
75 W Ar-MIP <sup>137</sup>	1.4 L/min Ar	ETV	405.8	10	500
170 W He-CMP*	10 L/min He	DSI	405.8	0.6	3

\*This Work.

Figure 4-13: Pb emission spectra for 10  $\mu\text{L}$  of 64 ppb Pb. The integration time is 0.18 s, and the monochromator slit width is 120  $\mu\text{m}$ .  
(TOP): Raw spectrum.  
(BOTTOM): Spectrum after using a filter to remove the fixed frequency noise.



## CHAPTER 5

### THE DETERMINATION OF LEAD IN WHOLE BLOOD BY DSI-CMP-AES

The primary goal of this research was to develop a method which would meet the requirements set by the Centers for Disease Control (Atlanta, GA) for a lead in whole blood screening technique. Those requirements entailed being able to determine lead in whole blood at a level of 100 ppb being within 10 % of the true value with a precision of 10 % or better. The detection limit of the method must be below 20 ppb. The sample size was limited to 200  $\mu$ L, and the analysis time per sample including sample preparation was limited to 5 minutes.<sup>139</sup>

#### Characterization of Whole Blood at 405 nm

For an analytical method to be useful, the analyte signal must be easily resolved from the background signal. In the case of emission, the Pb emission line should be well-resolved from neighboring emission lines. The background emission of whole blood was measured at 405 nm. The background emission lines were tentatively identified by their apparent wavelength. This wavelength was obtained by interpolation after the diode array had been calibrated with several aqueous standards. The identity of the background emission lines were confirmed by comparing the spectra obtained from aqueous standards to the spectra obtained from whole blood.

### Experimental

A 544 ppb (mass/mass) whole blood standard was prepared by adding approximately 0.5 mL of an aqueous 1 ppm Pb solution to 0.5 mL of a human whole blood sample using an air displacement pipette. Because blood proved difficult to transfer quantitatively, the actual concentration was determined by weighing the portions of the whole blood and the aqueous 1 ppm solution.

Five  $\mu\text{L}$  of this whole blood standard was deposited on the electrode using a positive displacement pipette. An air displacement pipette had been tested for this step also, but had exhibited a precision of 40 % for 10  $\mu\text{L}$  sample volumes while a positive displacement pipette had a much better precision of 9 % for 2  $\mu\text{L}$  sample volumes. The sample was dried for 90 s at 70 W. Following this step, helium was allowed to purge the torch at a flow rate of 10 L/min for 30 s. The power had been reduced to 13 W before the He flow had been initiated. The blood was then atomized and excited at a power of 170 W. The monochromator was operated with a narrow slit width of 20  $\mu\text{m}$  to ensure that most of the emission lines would be resolved.

Aqueous standards were prepared to help verify the identity of the background emission lines. These standards are identified in Table 5-1. The Ca, Mn, Fe, and K were obtained commercially in the form of atomic absorption standards. Copper was obtained as ACS grade copper sulfate and was dissolved in 5 % sulfuric acid. The sodium carbonate was obtained as ACS grade powder and was dissolved in distilled water.

## Results

The emission spectrum of whole blood from approximately 385 to 425 nm is shown in Figure 5-1. The CN bands are the most predominant feature in this wavelength region, and obscure the regions 386.2 - 388.3 nm, and 415.2 - 421.6 nm. Calcium presents the next strongest emission lines at 393.4, 396.8, and 422.7 nm. While these

Table 5-1 Aqueous Standards

Compound	Concentration
$\text{Ca}(\text{NO}_3)_2$	1 ppth* Ca
$\text{Mn}(\text{NO}_3)_2$	1 ppth Mn
$\text{Fe}(\text{NO}_3)_2$	250 ppm Fe
$\text{CuSO}_4$	1 ppth Cu
$\text{Na}_2\text{CO}_3$	10 %
$\text{KNO}_3$	1 ppth K

\* ppth = parts per thousand

emission lines are intense, they are far enough away from the Pb emission line at 405.8 nm that they do not spectrally interfere. Potassium emission lines at 404.4 nm and 404.7 nm are the strongest emission lines near Pb and present the greatest potential to interfere with the determination of lead. Figures 5-2 through 5-4 show spectra obtained from aqueous standards which were used to confirm the identity of these lines.

An expanded view of the whole blood spectrum is shown in Figure 5-5. The potassium peak has been truncated in order to show the lower intensity emission lines in greater detail. One can barely see the Pb signal at 405.8 nm. While K is the nearest spectral interferent at shorter wavelengths, Fe is the nearest spectral interferent at longer

Figure 5-1: Whole blood background emission at 405 nm. The monochromator slit width is 20  $\mu\text{m}$ .



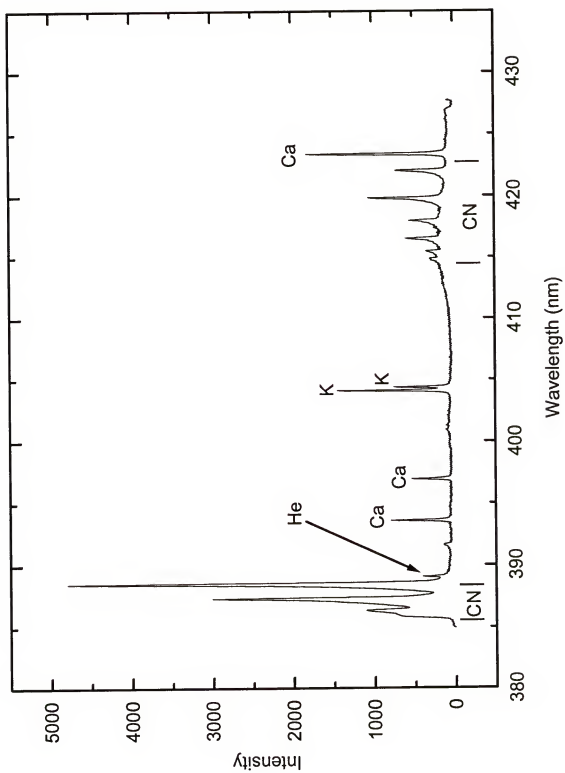


Figure 5-2: 1 ppb Ca emission spectrum. The monochromator slit width was 20  $\mu\text{m}$ .

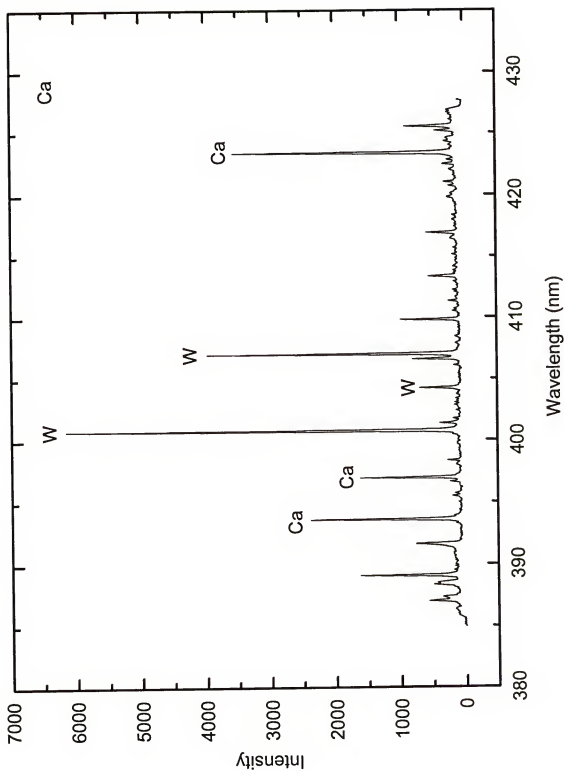


Figure 5-3: 1000 ppm K emission spectrum. The monochromator slit width was 120  $\mu\text{m}$ .

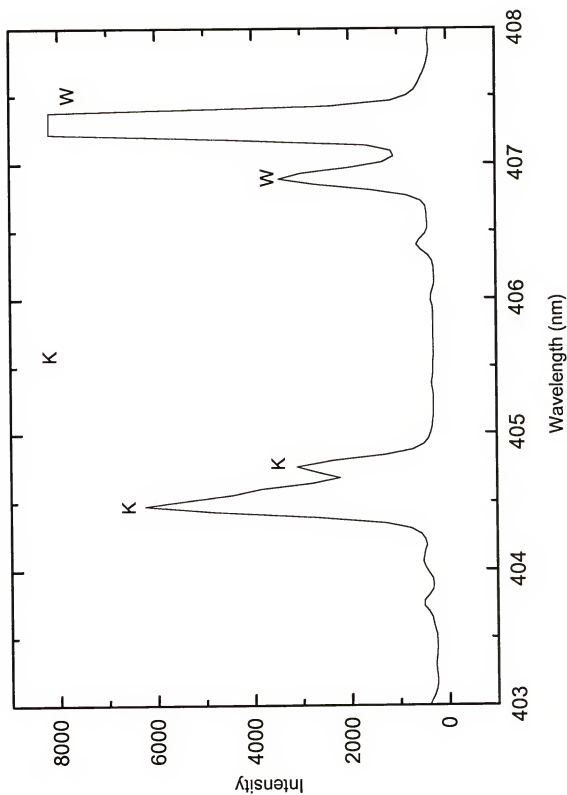


Figure 5-4: 10%  $\text{Na}_2\text{CO}_3$  emission spectrum. The monochromator slit width was  $120\text{ }\mu\text{m}$ .

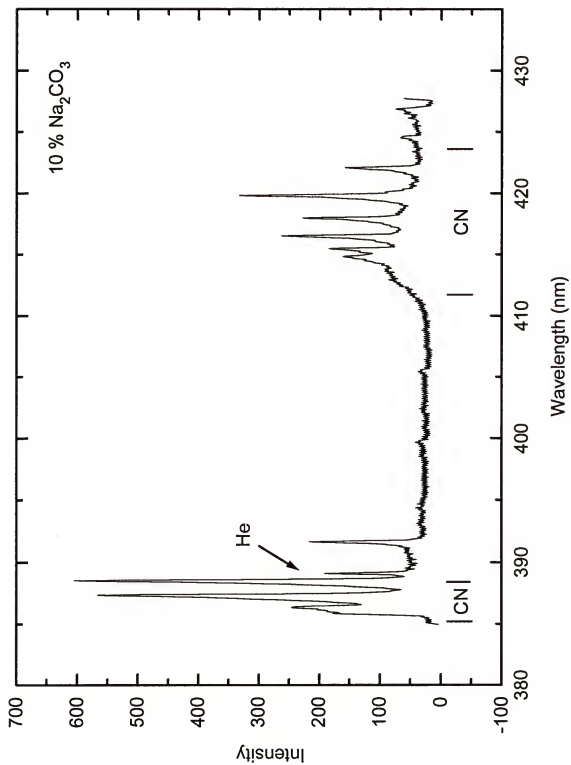
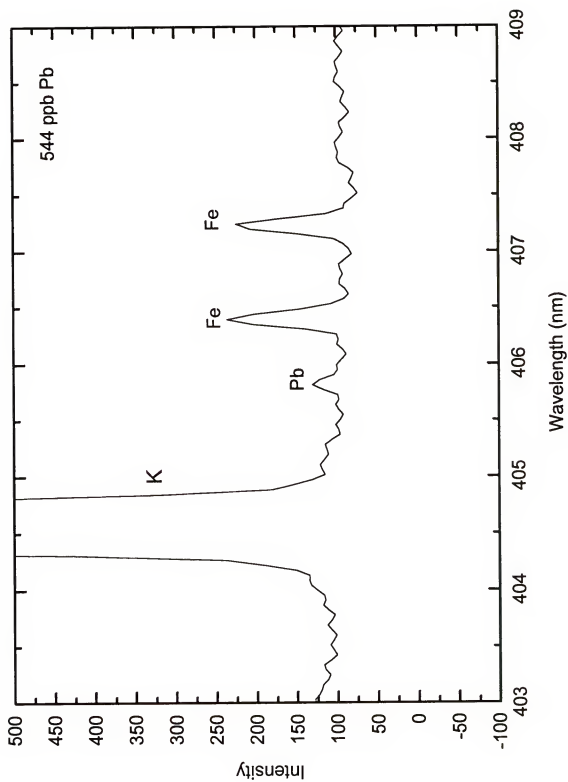


Figure 5-5: Expanded view of whole blood emission at 405 nm. Five  $\mu\text{L}$  of 544 ppb Pb was used. The monochromator slit width was 20  $\mu\text{m}$ .





wavelengths. An aqueous spectrum of 250 ppm Fe is shown in Figure 5-6, which shows Fe emission at 404.6 nm, 406.4 nm, and 407.2 nm. Iron is present in the human body at approximately 59 ppm.

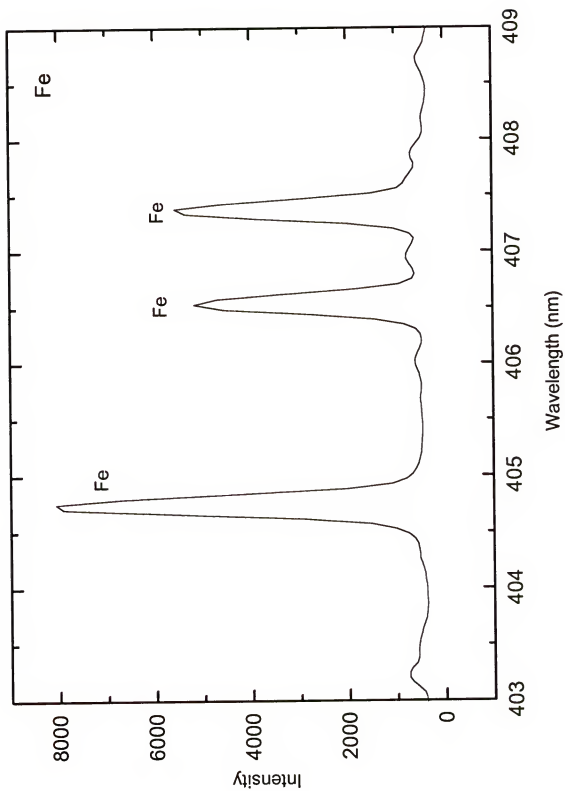
#### Characterization of the Plasma Ashing Step using Aqueous Samples

The amount of sample which enters the plasma during the atomization stage is critical. Introducing too much sample destabilizes the plasma and cools the plasma resulting in a lower signal for the analyte than otherwise would have been obtained. Electrothermal vaporization is typically the method of choice for introducing microliter volumes of samples into a plasma. The sample matrix is usually ashed, enriching the analyte and removing the more volatile portion of the matrix, prior to atomizing the analyte and the less volatile components of the matrix into the plasma. This work characterizes the use of a plasma-based ashing step in which heat from a low power plasma is responsible for ashing the sample matrix. Following this ashing step, the plasma power is increased and the analyte is atomized and excited. This technique benefits from the simplicity of not requiring electrothermal ashing.

#### Experimental

In order to assess the effectiveness of the ashing step, aqueous samples containing either potassium chloride, or lead chloride, or lead phosphate, were dried for 90 s, ashed at various plasma currents for a period of three minutes, and then atomized at approximately 170 W. Potassium and lead are present in whole blood in the form of the chloride salt. Lead phosphate was studied to compare the volatility of lead chloride and lead phosphate, and consequently whether a phosphate based matrix modifier would help

Figure 5-6: 250 ppm Fe Emission Spectrum. The monochromator slit width was 120  $\mu\text{m}$ .



retain more lead. In order to prepare the lead phosphate, 5  $\mu\text{L}$  of 0.2% phosphoric acid was added to 5  $\mu\text{L}$  of the lead chloride.

### Results

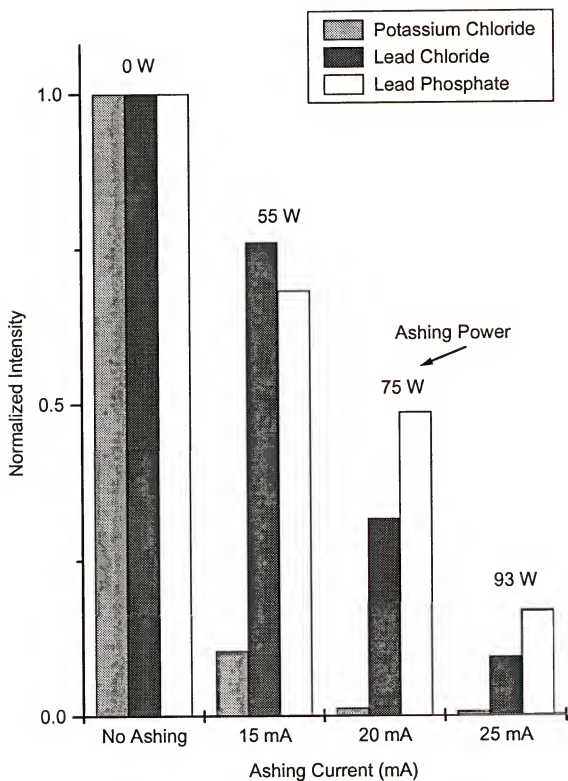
The resulting emission signals of potassium and lead were measured and normalized to the signals obtained when these solutions were dried and then directly atomized with no ashing step in-between. Therefore, the normalized emission signals represented the fraction of analyte remaining after the ashing step was employed. The results are shown in Figure 5-7. Lead phosphate should be less volatile than potassium chloride, and lead chloride should be the most volatile; however, this was not observed. Instead, the results for potassium chloride and lead chloride are reversed. This can be explained if air entrainment into the plasma converted the lead chloride to lead oxide during the ashing step; lead oxide is less volatile than potassium chloride.

The results show that some lead is lost in the ashing step. However, at an ashing current of 15 mA, 80 % of the lead remained, while only 20 % of the potassium remained. This current corresponded to an ashing power between 30 and 55 W. In order to obtain high sensitivity with discrimination of the K signal, an ashing current of 15 mA was used in further experiments.

### Radial and Axial Profiles

The radial and axial profiles of Pb emission from whole blood were measured to ensure that they were not significantly different from the aqueous profiles.

Figure 5-7: Ashing study of potassium chloride, lead chloride, and lead phosphate.



## Experimental

### Radial Profile

A whole blood standard was made by adding 0.3615 g of human whole blood to 0.8267 g of an aqueous 1 ppm Pb standard. This resulted in a 696 ppb (mass/mass) Pb standard.

### Axial Profile

A whole blood standard was made by adding 0.2712 g of human whole blood to 0.8002 g of an aqueous 1 ppm Pb standard. This resulted in a 747 ppb (mass/mass) Pb whole blood standard.

### Procedure

Five  $\mu\text{L}$  of the whole blood standard were deposited on the electrode. The whole blood was dried for 90 s at 70 W. The power was reduced to 14 W, and helium at a flow of 10 L/min was used to purge the torch for 30 s. The power was then increased to 170 W just after the detector was triggered. The monochromator was operated with a slit width of 120  $\mu\text{m}$ .

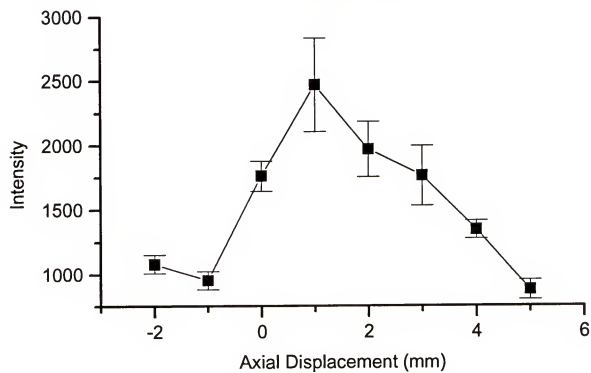
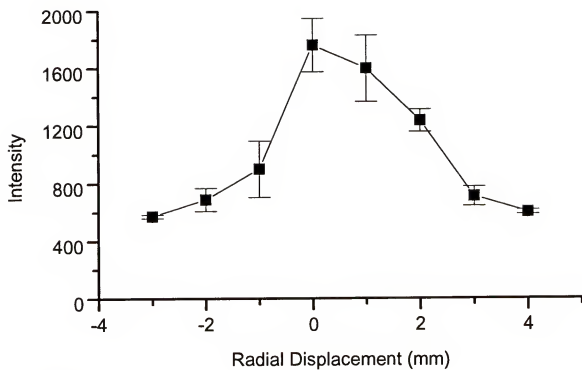
### Results

The results that were obtained are shown in Figure 5-8. The Pb signal is plotted versus the displacement from the center of the plasma for the radial profile. The Pb signal is plotted versus the displacement from the top of the electrode for the axial profile. Negative displacements correspond to positions below the electrode tip.

The Pb signal spatial profiles in whole blood are similar to the spatial profiles in aqueous samples. Alignment of the electrode is critical with respect to the optical axis.



Figure 5-8: Radial and axial profiles of lead in whole blood. The error bars correspond to one standard deviation ( $n=6$ ). 0 for the radial profile corresponds to the center of the plasma, while 0 for the axial profile corresponds to the top of the electrode.



One must be within 1 mm of the optimum intensity in order to obtain a reasonable signal to noise ratio. The optimum viewing distance is within 1 mm of the top of the electrode.

#### Optimization of the Ashing Time

The ashing power had been previously optimized using aqueous samples. This power was assumed to be the optimum for blood samples; however, the length of the ashing period still needed to be considered. If the ashing time was too low, an unstable plasma resulted during the atomization step, and if too long, needless loss of lead resulted.

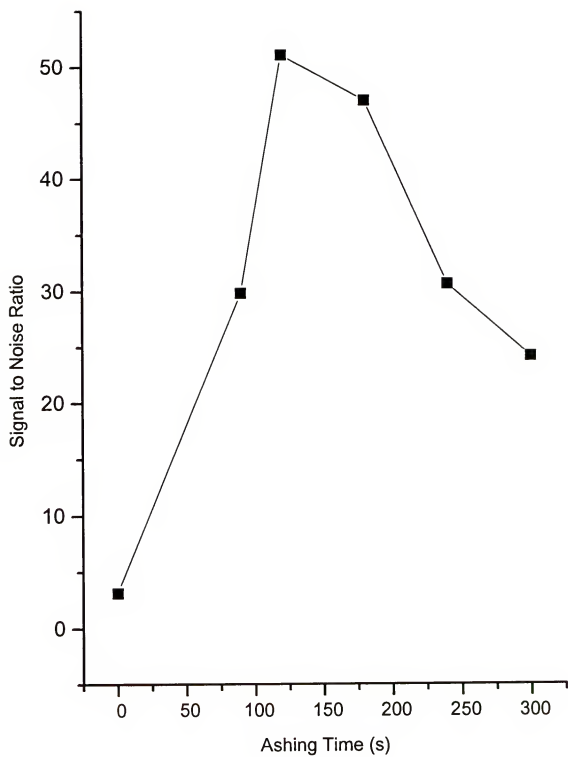
#### Experimental

The same 747 ppb Pb blood standard that was used in the axial profile experiment was used in this experiment. Five microliters of whole blood was placed onto the electrode and dried for 90 s at 70 W. After the drying step, the blood sample was ashed for a period of 0 s to 300 s, prior to the atomization step. For the 0 s ashing step, the power was reduced to 13 W, and helium was allowed to purge the torch for 30 s at 10 L/min. The power was then increased to 170 W for the atomization step. For the 30 s to 300 s ashing time, the power was reduced to 55 W after the drying step and He was introduced at 10 L/min. As soon as the He was introduced, a plasma ignited which ashed the sample. The power was then increased to 170 W for the atomization step.

#### Results

The Pb signal to noise ratio versus ashing time is plotted in Figure 5-9. At an ashing time of 0 s, the plasma was very unstable. The blood emission background was very intense and saturated the detector. In addition, manganese emission was observed

Figure 5-9: Pb signal to noise ratio versus the ashing time (s). 5  $\mu$ L of 747 ppb Pb was used.



at 405.6 nm and 405.9 nm (Figure 5-10) both of which could not be resolved from the lead peak. An aqueous spectrum of Mn is shown in Figure 5-11. As the ashing time increased, the manganese emission was no longer seen, and the potassium emission was greatly reduced. The optimum ashing time was two minutes, which resulted in the best signal to noise ratio for Pb. A spectrum which resulted from a two minute ashing time is shown in Figure 5-12.

#### Percent Recovery Study

A percent recovery study was performed to determine how free this method was from matrix effects. A whole blood lead standard was made which contained 3.33 ppm Pb, and this signal was compared to the signal obtained from an aqueous standard which contained 3.33 ppm Pb. The two signals were compared to determine if the presence of the blood matrix had an effect on the Pb signal.

#### Experimental

A 2 mL sample of whole blood was added to 1 mL of an aqueous 10 ppm Pb standard, which resulted in a 3.33 ppm Pb whole blood standard. A 2  $\mu$ L aliquot was deposited on the electrode, dried for 90 s at 70 W, ashed for 2 minutes at 55 W, and atomized at 170 W. An aqueous sample containing 3.33 ppm Pb was prepared from the 10 ppm Pb standard using the same dilution factor that was used with the whole blood. The aqueous sample was treated the same way as the blood sample, i.e. dried, ashed, and atomized for the same periods of time at the same powers.

Figure 5-10: Whole blood emission spectrum without ashing. Pb concentration = 747 ppb.  
Monochromator slit width = 120  $\mu\text{m}$ .

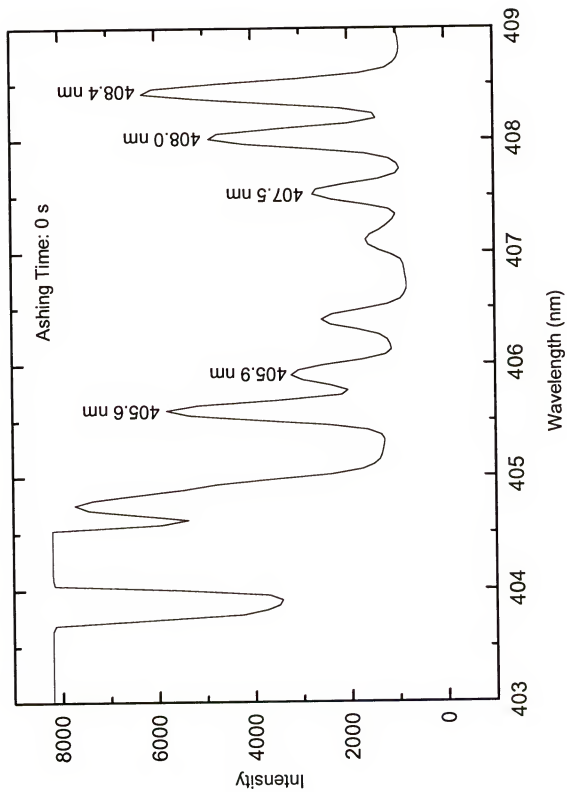




Figure 5-11: 1 ppb Mn emission spectrum. Monochromator slit width = 5  $\mu\text{m}$ .

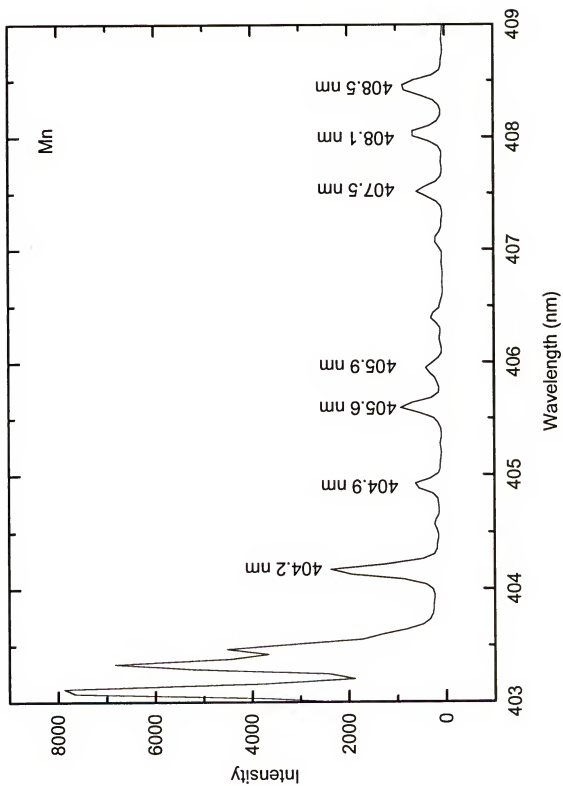
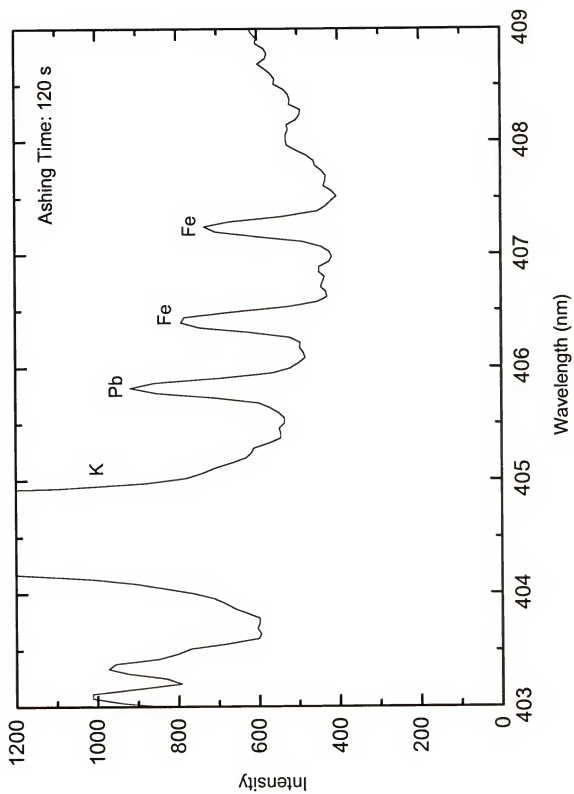


Figure 5-12: Whole Blood Emission Spectrum after ashing for 120 s. Pb concentration = 747 ppb. Monochromator slit width = 120  $\mu\text{m}$ .



## Results

The average temporal emission profile of Pb in blood is compared to the average profile of Pb in aqueous solutions in Figure 5-13. The Pb signal lasts longer in blood than in the aqueous sample. Also, the Pb signal was depressed in blood, although the % recovery, defined as the ratio the Pb signal in blood to the Pb signal in demineralized water, was 90%. Since the Pb signal is depressed in blood, matrix matched standards or the standard addition technique is required for calibration. The results of this experiment are shown in Table 5-2.

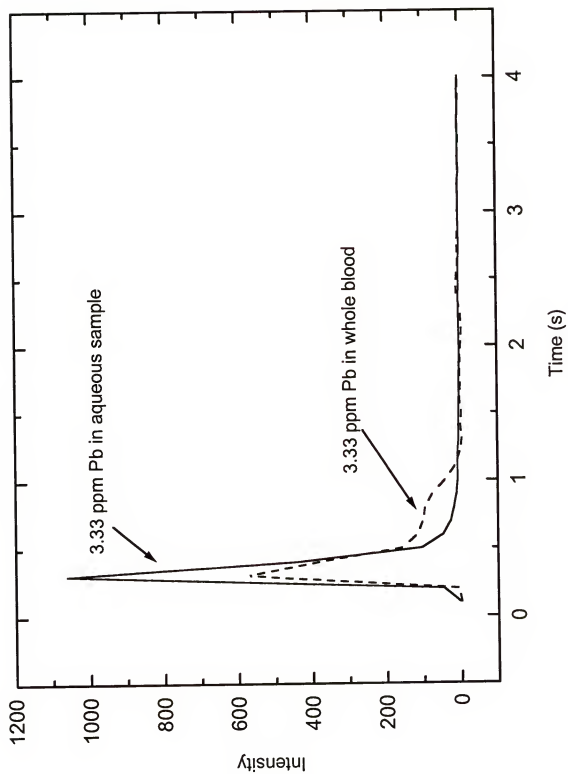
Table 5-2 Percent Recovery of Pb from Whole Blood

	Pb Signal	Standard Deviation	% RSD
Aqueous Sample	1728	93	5
Whole Blood Sample	1563	109	7
% Recovery	90 %		

## Determination of Accuracy

The accuracy of the CMP-AES method was determined using whole blood quality control materials (QCMs) which were available through the Centers for Disease Control (CDC) Blood Lead Laboratory Reference System. The method of standard additions was used along with these QCMs to determine the accuracy of this method.

Figure 5-13: Temporal profiles of aqueous and blood Pb standards.



## Experimental

### Preparation of Glassware

All glassware to be used was soaked in a 5 % nitric acid bath overnight. Following this, the glassware was rinsed with water provided by a Barnstead Nanopure system (Newton, MA). This whole procedure was then repeated to ensure that all lead in the glassware had been completely removed.

Pyrex pipettes were used to deliver whole blood into the 1 mL Pyrex glass test tubes which were used to contain the standard addition solutions. These pipettes were checked for accuracy and precision using standard gravimetric procedures. All the pipettes used in this experiment had a % RSD less than 0.7% and were at least within 3 % of their certified value.

### Procedure

Three CDC whole blood standards were analyzed; the blood standards contained 573 ppb, 188 ppb, and 48 ppb of lead, respectively. In the standard addition method, various volumes of an aqueous 1 ppm Pb solution were added to equal volumes of whole blood (0.2 mL). The solutions were then diluted with demineralized water to a total volume of 0.45 mL. The added Pb concentrations in the respective standard addition solutions are shown in Table 5-3 to Table 5-5. All components of each standard addition solution were weighed to ensure accuracy. In addition, after the solutions were prepared, they were sonicated for 5 minutes to ensure complete mixing between the blood and aqueous components.



Table 5-3 573 ppb Whole Blood Standard\*

Solution	Volume of Blood	Mass of Blood	Volume of 1 ppm Pb	Mass of 1 ppm Pb	Volume of Water	Mass of Water	Total Volume	Final Conc. Pb Added
1	0.2	0.2069	0	0	0.25	0.2594	0.45	0
2	0.2	0.2086	0.05	0.0508	0.20	0.2097	0.45	111
3	0.2	0.2064	0.15	0.1625	0.10	0.1042	0.45	333
4	0.2	0.2065	0.25	0.2650	0	0	0.45	556

\* All masses are in g.  
 All volumes are in mL.  
 All concentrations are in ppb.

Table 5-4 188 ppb Whole Blood Standard\*

Solution	Volume of Blood	Mass of Blood	Volume of 1 ppm Pb	Mass of 1 ppm Pb	Volume of Water	Mass of Water	Total Volume	Final Conc. Pb Added
1	0.2	0.2123	0	0	0.25	0.2643	0.45	0
2	0.2	0.2131	0.15	0.1578	0.10	0.1058	0.45	333
3	0.2	0.2118	0.25	0.2618	0	0	0.45	556

\* All masses are in g.

All volumes are in mL.

All concentrations are in ppb.

Table 5-5 48 ppb Whole Blood Standard\*

Solution	Volume of Blood	Mass of Blood	Volume of 1 ppm Pb	Mass of 1 ppm Pb	Volume of Water	Mass of Water	Total Volume	Final Conc. Pb Added
1	0.2	0.2003	0	0	0.25	0.2621	0.45	0
2	0.2	0.2001	0.05	0.0505	0.20	0.2225	0.45	111
3	0.2	0.1997	0.15	0.1538	0.10	0.1064	0.45	333
4	0.2	0.2044	0.25	0.2598	0	0	0.45	556

\* All masses are in g.

All volumes are in mL.

All concentrations are in ppb.

The Pb in the solutions were analyzed by depositing 5  $\mu\text{L}$  onto the electrode. The solution was dried at 70 W for 90 s. Following this, the power was decreased to approximately 55 W, and the helium flow was initiated at 10 L/min. When the helium was added, a plasma ignited, and the sample was ashed for a period of two minutes. The power was then increased to 170 W, and the lead emission was measured. The diode array was triggered just prior to the increase in power to 170 W. After the diode array was triggered it was read out every 0.18 s, a total of 40 times and the time resolved lead signal was obtained. A 1 minute cleanout step was necessary after the atomization step to remove residual carbon. The plasma was operated at a power of 200 W and 100 mL/min of  $\text{H}_2$  was added to the helium.

## Results

### Signal Analysis

The raw spectrum was background subtracted by taking the first derivative of the signal. Figure 5-14 shows a spectrum of 83.5 ppb Pb and its first derivative. The first derivative acts as a high pass filter, as it accentuates high frequencies and attenuated lower frequencies. Several authors have reported using the first derivative. Two excellent papers on this topic are those by O'Haver<sup>140</sup> and by Savitzky and Golay<sup>141</sup>. Spectrally narrower peaks usually associated with atomic emission lines are accentuated over the wider peaks associated with molecular emission and the curved baseline associated with continuum emission. The first derivative plot presented in Figure 5-14 shows an average background signal of zero, showing the effectiveness of the first derivative for background correction. The lead signal was obtained as shown in

Figure 5-14: (TOP):  
(BOTTOM):

Raw spectrum of 83.5 ppb Pb in whole blood.  
First derivative of raw spectrum.

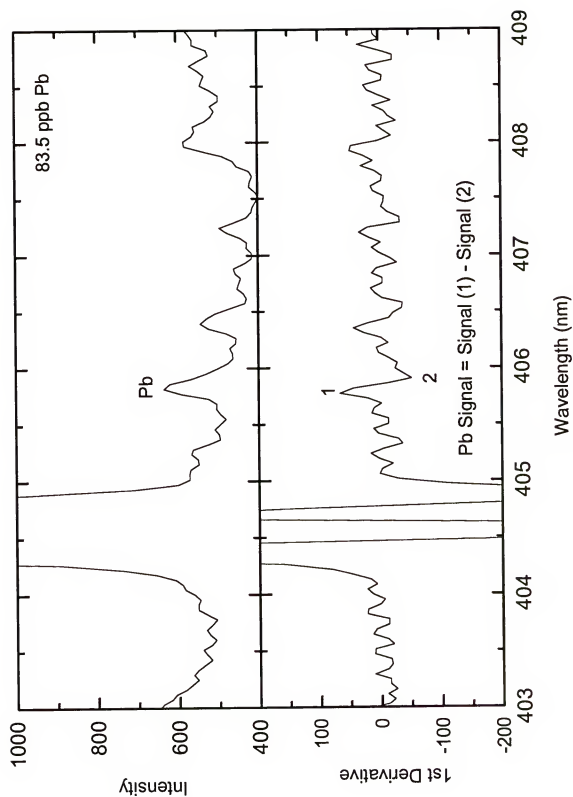


Figure 5-14 by subtracting the maximum value of the first derivative of the lead peak from the minimum value. This corresponded to the measurement of peak height in the original spectrum.

The spectrum shown in Figure 5-14 represents an integration time of 0.18 s (i.e. a single spectrum of the 40 time resolved spectra collected) where the Pb signal was greatest. The time resolved Pb signal of a blood sample containing 665 ppb Pb is shown in Figure 5-15. Due to the variation in the shapes of these temporal profiles from run to run, a longer integration time resulted in better precision. Peak area proved to be more precise than peak height. A plot of the precision versus the integration time is shown in Figure 5-16 for a Pb concentration of 665 ppb. The Pb signal was obtained by starting with the peak height signal and successively adding Pb signals on either side of peak height signal in time; this was analogous to centering the gate of a boxcar averager on the peak signal and widening the gate. A total of 5 runs were compared and the relative standard deviation was determined. The optimum % RSD was obtained when the Pb signal was integrated for a 1.98 s interval: from time 0 to 1.98 s. This integration time was used for all the CDC whole blood standards.

The noise on each signal was determined by measuring the fluctuation in the signal level after the lead was gone. More precisely, the noise was determined by measuring the standard deviation of the signal level over the time period from 5.4 s to 7.2 s. By this time all the lead was gone, and the noise in the background level was being measured. Figure 5-17 shows a temporal emission plot of 83.5 ppb Pb in whole

Figure 5-15: Temporal emission profile of 665 ppb Pb in whole blood.



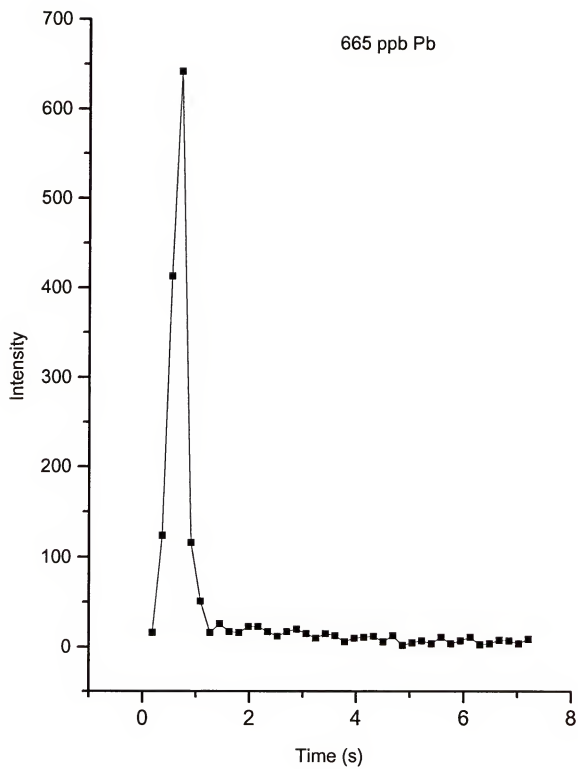


Figure 5-16: Precision of the Pb emission signal versus the integration time.

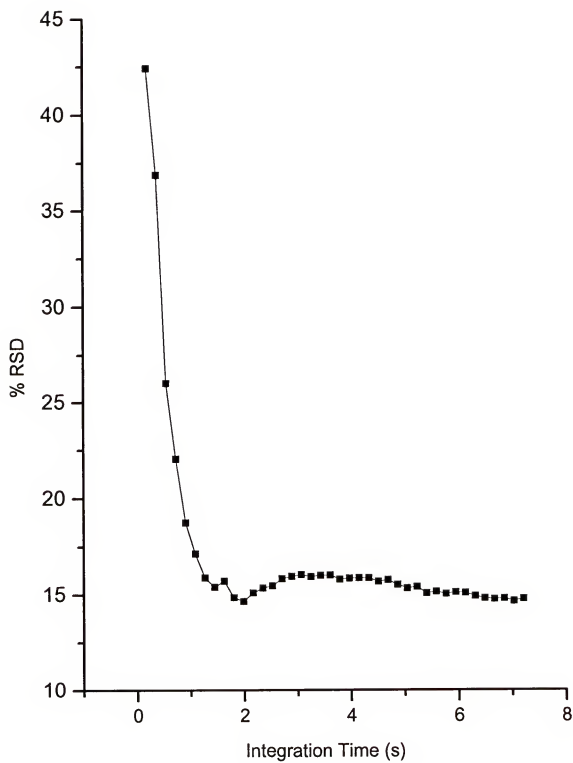
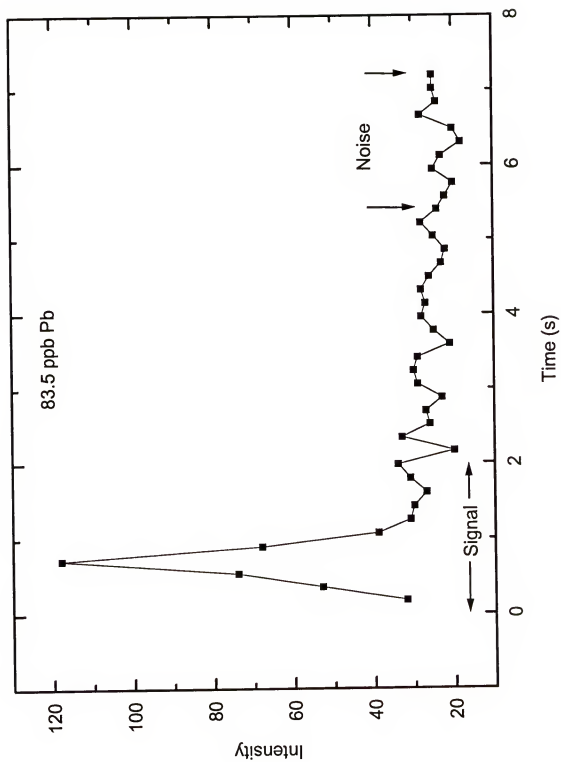


Figure 5-17: Temporal Emission Profile of 83.5 ppb Pb in whole blood.



blood; the signal and the noise region are identified. Figure 5-18 shows a plot of the 83.5 ppb Pb signal in the wavelength domain after the background has been subtracted.

#### Analytical Figures of Merit

The results of the standard addition analysis are shown in Table 5-6. A t-test was used to determine if the measured concentration was significantly different from the actual concentration at the 95 % confidence level. In the case of the 573 ppb and 188 ppb standards, there was no significant difference between the measured and actual concentrations. However, the predicted value for the 48 ppb standard was 81 % too high. Sample contamination could have resulted in a higher value.

The overall precision was determined by averaging the precisions obtained for every sample run. In total this represented 55 runs. The average precision was approximately 15%. The CDC requires an average precision of less than 10% for a screening technique. The precision was limited by sample loading of the plasma. The precision could be lowered by increasing the plasma power, decreasing the sample size, or using an internal standard which behaved similarly to Pb during the ashing and atomization stages.

The detection limit calculated based on 3 standard deviations of the background signal was 7 ppb. For a sample size of 5  $\mu$ L, this corresponds to an absolute detection limit of 35 pg. This CMP-AES method meets the detection limit required by the CDC for a screening technique. In addition, the detection limit is comparable to that achieved by graphite furnace atomic absorption spectrometry (9 pg).<sup>142</sup> The analysis time per

Figure 5-18: Emission spectrum of 83.5 ppb Pb in whole blood after background subtraction. A monochromator slit width of 120  $\mu\text{m}$  was used.

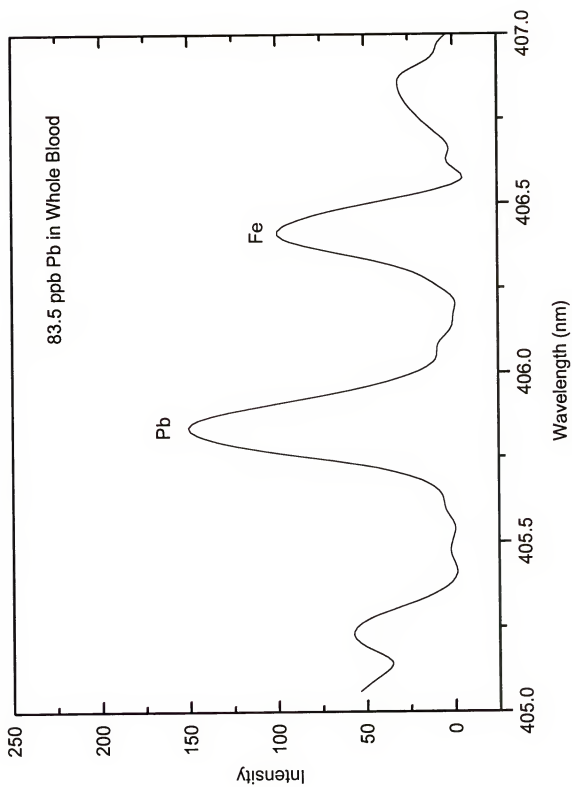




Table 5-6 Accuracy of the Whole Blood Determinations

Actual Concentration (ppb)	Measured Concentration (ppb)	% Difference
573	661 $\pm$ 91	+ 15
188	194 $\pm$ 19	+ 3
48	90 $\pm$ 13	+ 81

sample including the cleanup step was just below 5 minutes, and also meets the requirements set by the CDC.

This CMP-AES method compares favorably with other AES techniques. Few workers have reported figures of merit for the determination of lead in whole blood. The results obtained by various investigators are shown in Table 5-7. The CMP-AES method compares well with the two ETV-ICP-AES techniques in terms of precision and accuracy. Both CMP-AES and ETV-ICP techniques are very rapid. The best precision is obtained when sample pretreatment is employed as is shown with the DC arc and ICP-AES methods listed at the end of Table 5-7. However, the analysis time is too long to be considered for screening purposes.

#### Conclusions

The CMP-AES method for the determination of lead in whole blood meets the requirements of the CDC for a screening method in terms of the detection limit and the analysis time. However, the accuracy and precision of the technique still needs to be improved. This presumably could be accomplished by reducing the sample size, increasing the plasma power, or by ratioing the lead signal against that of an appropriate internal standard.

Table 5-7: Figures of Merit for Pb in Whole Blood obtained with AES

Plasma	Sample Introduction Method/ Treatment	Analysis Time/ Sample	Pb Concentration (ppb)	Accuracy	Precision
Ar-ICP <sup>91</sup>	ETV, 30 s ashing stage	< 2 min	460	2 - 15 %	Not Reported
			290	3 - 14 %	Not Reported
Ar-ICP <sup>18</sup>	ETV, no ashing stage	< 1 min	48	4 %	13 % (n=3)
			113	10 %	29 % (n=3)
			187	25 %	11 % (n=3)
DC Arc <sup>30</sup>	Removal of Proteins, Removal of Alkali and Alkaline Earth Metals, Thermal Ashing, Preconcentration	> 4 hrs	62	3 %	Not Reported
Ar-ICP <sup>34</sup>	Removal of Proteins, Removal of Alkali and Alkaline Earth Metals, 12 hr Thermal Ashing, Removal of Fe, Preconcentration Step, Pneumatic Nebulization	> 12 hrs	410	3 %	3 % (n=6)
			735	4 %	2 % (n=6)

## CHAPTER 6 CONCLUSIONS AND FUTURE WORK

### Summary of Results

The detection limits determined for lead using the capacitively coupled microwave plasma atomic emission spectrometer in both aqueous and whole blood samples was very good. A detection limit of 0.6 ppb Pb was obtained for a 5  $\mu$ L aqueous sample (absolute detection limit: 3 pg). In addition, a detection limit of 4 ppb for a 5  $\mu$ L blood sample was obtained (absolute detection limit: 20 pg). These represent the best detection limits for Pb by CMP-AES to date. The instrument yielded promising results, but does not yet meet all the requirements set by the CDC for a lead in blood screening technique. The accuracy at levels of 48 ppb is questionable. The reason for this should be determined. However, good accuracy was achieved for blood lead levels above 100 ppb. The precision of this method at 15 % does not meet the CDC's requirements either. However, the precision is close to the CDC's requirement of 10 %; and future work may yet improve the accuracy and precision of the technique.

### Future Work

#### Nickel Cups

The precision and the accuracy of the method could be improved by changing the electrode from the tungsten wire to a nickel cup, similar in design to the graphite cup used by Ali and Winefordner.<sup>143</sup> The cup would be in place in the central channel of

the torch by a supporting metal electrode. Nickel is advantageous over graphite in that refractory compounds such as carbides do not form. In addition, the smaller pore size of nickel, and metals in general, reduces the memory effects that have been associated with graphite. Nickel is advantageous over tungsten since it does not oxidize as easily. Oxygen could then be added during the blood ashing stage to ensure the complete oxidation of lead. Since lead oxide is less volatile than lead chloride, a larger emission signal should result. Another benefit of the metal cups is their greater sample capacity, 20 - 50  $\mu\text{L}$ , compared to the tungsten filament, 10  $\mu\text{L}$ . Because of this, lower concentration detection limits should result. Nickel cups have been tested in a CMP by the author and have been able to withstand high powers (> 600 W) from the CMP. This is in contrast to the 0.25 mm nickel filament which melted at 170 W. Because of the higher powers that can be used this plasma should be less affected by the blood matrix. Nickel cups have also been tested by this author, and they couple well to the microwave field. Plasmas can be sustained at powers as little as 55 W, similar to the tungsten filament electrode.

#### Matrix Modifiers

The addition of matrix modifiers, in particular, diammonium hydrogen phosphate should be studied. With this modifier lead chloride would be converted into lead phosphate. Although the use of matrix modifiers inevitably involves greater sample handling and dilution, if more lead could be retained during the blood ashing step an enhancement in the lead signal should result.

### Feedback Regulation of the Ashing Step

The ashing step is regulated only by using a current-regulated power supply to maintain the same current in the plasma. Ideally, regulation of the plasma temperature should be maintained. This could be done as it is done in electrothermal vaporizers, by measuring the temperature of the cup or wire with an optical pyrometer, and using this parameter to regulate the power supply.

### Other Thermal Ashing Techniques

In principal, plasma ashing is the simplest form of thermal ashing that could be used with CMP-AES, as it requires no other devices. However, this type of ashing has been studied very sparsely. Other ashing techniques could be coupled to the electrode. The electrode could be resistively heated with a dc voltage or inductively heated with an RF field, the latter has the advantage of not requiring any physical connections.

### Redesign of the Plasma Torch

The plasma torch needs to be redesigned so that it can be purged more efficiently, requiring lower helium flow rates. At present, the torch is shielded from the atmosphere only with a quartz tube, the "quartz chimney", which lies on top of the waveguide. The chimney is concentric with the torch, has an inner diameter of 33 mm and an length of 62 mm. The top part of the cylinder is not sealed, but instead exposed to the atmosphere. To reduce the extensive dead volume of this system, the plasma torch length could be shortened to 3/4 its present length, from 15 cm to 11 cm. This would reduce the volume of the torch by 1/4. In addition, the quartz chimney top be sealed with a metal lid. Incorporated into this lid should be a check valve which vents at a

specific pressure. In this way the valve would only open when the pressure of the gas inside the chimney was greater than the pressure of the atmosphere around it. This should be very effective in reducing the amount of helium which must be used to purge the torch, should be very simple to construct, and should be very cost-effective.

Discrete sample introduction capacitively coupled microwave atomic emission spectroscopy (DSI-CMP-AES) is a very sensitive method comparable in detection power to ICP-AES at a fraction of the cost. Its potential has been under-utilized and should be investigated further.

## REFERENCES

1. U.S. Centers for Disease Control (CDC). *Preventing Lead Poisoning in Young Children: A Statement by the Center for Disease Control in October, 1991*. U.S. Department of Health and Human Services/Public Health Service/Centers for Disease Control: Atlanta, GA, 1991; p. 1.
2. U.S. Department of Housing and Urban Development (HUD). *Comprehensive and Workable Plan for the Abatement of Lead-based Paint in Privately Owned Housing: Report to Congress*. HUD: Washington, D.C., 1990.
3. Noble, D. *Analytical Chemistry* **1993**, 65, 267A.
4. Patterson, C.C.; Settle, D.M. *SEAREX Newsletter* **1987**, 10, 1.
5. Pacyna, J.M.; Nriagu, J.O. *Nature* **1988**, 333, 134.
6. Schrier, L.C.; Manahan, S.E. *Spectroscopy* **1994**, 9, 24.
7. Mushak, P.; Davis, J.M.; Crocetti, A.F.; Grant, L.D. *Environmental Research* **1989**, 50, 11.
8. Boeckx, R.L. *Analytical Chemistry* **1986**, 58, 274A.
9. Agency for Toxic Substances and Disease Registry (ATSDR). *Case Studies In Environmental Medicine: Lead Toxicity*. ATSDR: Atlanta, GA, 1990.
10. U.S. Centers for Disease Control (CDC). *Preventing Lead Poisoning in Young Children: A Statement by the Center for Disease Control in October, 1991*. U.S. Department of Health and Human Services/Public Health Service/Centers for Disease Control: Atlanta, GA, 1991; p. 51.
11. U.S. Environmental Protection Agency (EPA). *Report of the Clean Air Scientific Advisory Committee: Review of the QAQPS Lead Staff Paper and the ECAO Air Quality Criteria Document Supplement*. Clean Air Scientific Advisory Committee, Scientific Advisory Board. U.S. EPA: Washington, D.C., 1990.
12. Nuttall, K.L.; Gordon, W.H.; Ash, K.O. *Clinical Chemistry* **1993**, 6, 1349.



13. Minoia, C.; Sabbioni, E.; Apostoli, P.; Pietra, R.; Pozzoli, L.; Gallorini, M.; Nicolaou, G.; Alessio, L.; Capodaglio, E. *The Science of the Total Environment* **1990**, *95*, 89.
14. Schroeder, H. A. *Journal of Chronic Diseases* **1965**, *18*, 217.
15. Everson, J.; Patterson, C.C. *Clinical Chemistry* **1980**, *26*, 1603.
16. Sabbioni, E.; Minoia, C.; Pietra, R.; Fortaner, S.; Gallorini, C.; Saltelli, A. *The Science of the Total Environment* **1992**, *120*, 39.
17. Delves, H.T.; Campbell, M.J. *Journal of Analytical Atomic Spectrometry* **1988**, *3*, 343.
18. Blakemore, W.M.; Casey, P.H.; Collie, W.R. *Analytical Chemistry* **1984**, *56*, 1376.
19. Heltai, Gy.; Broekaert, J.A.C.; Burba, P.; Leis, F.; Tschopel, P.; Tolg, G. *Spectrochimica Acta* **1990**, *45B*, 857.
20. Subramanian, K.S. *Progress in Analytical Atomic Spectroscopy* **1986**, *9*, 237.
21. Delves, H.T. *Progress in Analytical Atomic Spectroscopy* **1981**, *4*, 1.
22. Roda, S.M.; Greenland, R.D.; Bornschein, R.L.; Hammond, P.B. *Clinical Chemistry* **1988**, *34*, 563.
23. Aguilera de Benzo, Z.; Fraile, R.; Carrion, N.; Loreto, D. *Journal of Analytical Atomic Spectrometry* **1989**, *4*, 397.
24. Pleban, P.A.; Pearson, K.H. *Analytical Letters* **1979**, *12B*, 935.
25. Miller, D.T.; Paschal, D.C.; Gunter, E.W.; Stroud, P.E.; D'Angelo, J. *Analyst* **1987**, *112*, 1701.
26. Brown, A.A.; Halls, D.J.; Taylor, A. *Journal of Analytical Atomic Spectrometry* **1987**, *2*, 43R.
27. Navarro, J.A.; Granadillo, V.A.; Parra, O.E.; Romero, R.A. *Journal of Analytical Atomic Spectrometry* **1989**, *4*, 401.
28. Skelding, D.; Hodges, D.J. *Analyst* **1983**, *108*, 813.
29. Willard, H.H.; Merritt, Jr., L.L.; Dean, J.A.; Settle, JR., F.A. *Instrumental Methods of Analysis*, 7th ed.; Wadsworth, Inc.; Belmont, CA, 1988; p. 719.

30. Troshkova, G.P.; Yudelevich, I.G. *Journal of Analytical Chemistry of the USSR* **1990**, *45*, 899.
31. Yudelevich, I.G.; Troshkova, G.P. *Analisis* **1992**, *20*, 341.
32. Marinov, M.I. *Fresenius' Zeitschrift fuer Analytische Chemie* **1984**, *319*, 317.
33. Schramel, P. *Spectrochimica Acta* **1988**, *43B*, 881.
34. van Deijck, W.; Lips, M.J.; Maessen, F.J.M.J. *Fresenius' Zeitschrift fuer Analytische Chemie* **1984**, *317*, 858.
35. Hanamura, S.; Smith, B.W.; Winefordner, J.D. *Canadian Journal of Spectroscopy* **1984**, *29*, 13.
36. Fassel, V.A. *Science* **1978**, *202*, 183.
37. Boumans, P.W.J.M. *Fresenius' Zeitschrift fuer Analytische Chemie* **1979**, *299*, 341.
38. Greenfield, S.; Jones, I. Ll.; McGeachin, H. McD.; Smith, P.B.; *Analytica Chimica Acta* **1975**, *74*, 234.
39. Montaser, A.; Fassel, V.A. *Analytical Chemistry* **1976**, *48*, 1492.
40. Kenkel, J. *Analytical Chemistry: Refresher Manual*; Lewis Publishers: Boca Raton, FL, 1992; p. 191.
41. Fassel, V.A. *Proceedings of the 16th Colloquium Spectroscopicum Internationale*, Heidelberg 1971, Plenary lectures and reports: Adam Hilger, London, England, 1972; p. 63.
42. Greenfield, S.; McGeachin, H., McD.; Smith, P.B. *Talanta* **1976**, *23*, 1.
43. Greenfield, S.; Jones, I.Ll., McGeachin, H.McD.; Smith, P.B. *Analytica Chimica Acta* **1975**, *74*, 225.
44. Lajunen, L.H.J. *Spectrochemical Analysis By Atomic Absorption and Emission*; The Royal Society of Chemistry: Cambridge, England, 1992; p. 158.
45. Decker, R.J. *Spectrochimica Acta* **1980**, *35B*, 19.
46. Applied Research Laboratories *Spectraspan 7 DCP* **1994**.
47. Beenakker, C.I.M. *Spectrochimica Acta* **1976**, *31B*, 485.

48. Zander, A.T.; Hieftje, G.M. *Applied Spectroscopy* **1981**, *35*, 357.
49. Goode, S.R.; Baughman, K.W. *Applied Spectroscopy* **1984**, *38*, 755.
50. Fehsenfeld, F.C.; Evenson, K.M.; Broida, H.P. *Review of Scientific Instrumentation* **1965**, *36*, 294.
51. Long, G.L.; Perkins, L.D. *Applied Spectroscopy* **1987**, *41*, 980.
52. Cull, K.B.; Carnahan, J.W. *Applied Spectroscopy* **1988**, *42*, 1061.
53. Cull, K.B.; Carnahan, J.W. *J. Microwave Power Electromagnetic Energy* **1989**, *24*, 151.
54. Haas, D.L.; Caruso, J.A. *Analytical Chemistry* **1984**, *56*, 2014.
55. Ebdon, L.; Hill, S.; Ward, R.W. *Analyst* **1986**, *111*, 1113.
56. Uden, P.C. *Chromatographic Forum* **1986**, *5*, 17.
57. Quimby, B.D.; Sullivan, J.J. *Analytical Chemistry* **1990**, *62*, 1027.
58. Gelhausen, J.M.; Carnahan, J.W. *Applied Spectroscopy* **1991**, *63*, 2430.
59. Michlewicz, K.G.; Carnahan, J.W. *Analytical Letters* **1987**, *20*, 1193.
60. Webster, G.K.; Carnahan, J.W. *Applied Spectroscopy* **1991**, *45*, 1285.
61. Alvarado, J.; Carnahan, J.W. *Applied Spectroscopy* **1993**, *47*, 2036.
62. Wu, Mingin; Carnahan, J.W. *Journal of Analytical Atomic Spectrometry* **1992**, *7*, 1249.
63. Alvarado, J.; Wu, M.; Carnahan, J.W. *Journal of Analytical Atomic Spectrometry* **1992**, *7*, 1253.
64. Cobine, J.D.; Wilbur, D.A. *Journal of Applied Physics* **1951**, *22*, 835.
65. Cobine, J.D.; Wilbur, D.A. *Electronics* **1951**, *24*, 92.
66. Schmidt, W. *Elektronische Rundschau* **1959**, *13*, 404.
67. Mavrodineau, R.; Hughes, R.C. *Spectrochimica Acta* **1963**, *19*, 1309.
68. Masamba, W.R.L. Dissertation, University of Florida, 1992.
69. Kessler, W.; Gebhardt, F. *Glastechnische Berichte* **1971**, *44*, 483.

70. Suzuki, M. *Bunseki Kagaku* **1968**, *17*, 1529.
71. Masamba, W.R.L.; Smith, B.W.; Winefordner, J.D. *Applied Spectroscopy* **1992**, *46*, 1741.
72. Aziz, A.; Broekaert, J.A.C.; Leis, F. *Spectrochimica Acta* **1982**, *37B*, 369.
73. Uchida, H.; Nojiri, Y.; Haraguchi, H.; and Fuwa, K. *Analytica Chimica Acta* **1981**, *123*, 57.
74. Kleinman, I.; Svoboda, V. *Analytical Chemistry* **1969**, *41*, 1029.
75. Gunn, A.M.; Millard, D.C.; Kirkbright, G.F. *Analyst* **1978**, *103*, 1066.
76. Gunn, A.M.; Millard, D.C.; Kirkbright, G.F. *Analyst* **1980**, *5*, 502.
77. Cope, M.J.; Kirkbright, G.F.; Burr, P.M. *Analyst* **1982**, *107*, 611.
78. Barnett, N.W.; Chen, L.S.; Kirkbright, G.F. *Analytica Chimica Acta* **1983**, *149*, 115.
79. Kirkbright, G.F.; Snook, R.D. *Analytical Chemistry* **1979**, *51*, 1938.
80. Snook, R.D.; Kirkbright, G.F. *Applied Spectroscopy* **1983**, *37*, 11.
81. Ng, K.C.; Caruso, J.A. *Analytica Chimica Acta* **1982**, *143*, 209.
82. Ng, K.C.; Caruso, J.A. *Analyst* **1983**, *108*, 476.
83. Ng, K.C.; Caruso, J.A. *Analytical Chemistry* **1983**, *55*, 1513.
84. Ng, K.C.; Caruso, J.A. *Analytical Chemistry* **1983**, *55*, 2032.
85. Hirato, T.; Akagi, T.; Shimizu, H.; Masuda, A. *Analytical Chemistry* **1989**, *61*, 2263.
86. Nixon, D.E.; Fassel, V.A. , and Kniseley, R.N. *Analytical Chemistry* **1974**, *46*, 210.
87. Kitazume, E. *Analytical Chemistry* **1983**, *55*, 802.
88. Hartenstein, S.D.; Swaidan, H.M.; Christian, G.D. *Analyst* **1984**, *108*, 1323.
89. Swaidan, H.M.; Christian, G.D. *Analytical Chemistry* **1984**, *56*, 120.
90. Tikkanen, M.W.; Niemczyk, T.M. *Analytical Chemistry* **1986**, *58*, 266.

91. Alvarado, J.; Cavalli, T.; Omenetto, N.; Rossi, G.; Ottaway, J.M. *Journal of Analytical Atomic Spectrometry* **1987**, *2*, 357.
92. Dean, J.R.; Snook, R.D *Journal of Analytical Atomic Spectrometry* **1986**, *1*, 461.
93. Salin, E.D.; Horlick, G. *Analytical Chemistry* **1979**, *51*, 2284.
94. Walton, S.J.; Kirkbright, G.F. *Analyst* **1982**, *107*, 276.
95. Kirkbright, G.F.; Li-Xing, Z. *Analyst* **1982**, *107*, 617.
96. Li-Xing, Z.; Kirkbright, G.F.; Cope, M.J.; Watson, J.M. *Applied Spectroscopy* **1983**, *37*, 250.
97. Chan, W.T.; Horlick, G. *Applied Spectroscopy* **1990**, *44*, 380.
98. Greenfield, S. *Industrial Research and Development* **1981**, *23*, 140.
99. Greenfield, S. *Spectrochimica Acta* **1983**, *38B*, 93.
100. Gallego, M.; Lague de Castro, M.D; Valcaral, M. *Atomic Spectroscopy* **1985**, *6*, 16.
101. McLeod, C.W.; Worsfold, P.J.; Cox, A.G. *Analyst* **1984**, *109*, 327.
102. Jacintho, A.O.; Zagatto, E.A.G.; Bergamin, F.H.; Krug, F.J.; Reis, B.F.; Bruns, R.E.; Kowalski, B.R. *Analytica Chimica Acta* **1983**, *130*, 243.
103. Zagatto, E.A.G.; Jacintho, A.O.; Krug, F.J.; Reis, B.F.; Bruns, R.E.; Araujo, M.C.A. *Analytica Chimica Acta* **1983**, *145*, 169.
104. Gine, M.F.; Krug, F.J.; Filho, H.B.; dos Reis, B.F.; Zagatto, E.A.G.; Burns, R.E. *Journal of Analytical Atomic Spectrometry* **1988**, *3*, 673.
105. Moore, G.L.; Watson, A.E.; Humphries-Cuff, P. *Spectrochimica Acta* **1982**, *37B*, 835.
106. Long, S.E.; Snook, R.D. *Analyst* **1983**, *108*, 1331.
107. Pretty, J.F.; Evans, E.H.; Blubaugh, E.A.; Shen, W.L., Caruso, J.A.; Davidson, T.M. *Journal of Analytical Atomic Spectrometry* **1990**, *5*, 437.
108. Liversage, R.R.; Van Loon, J.C.; De Andrade, J.C. *Analytica Chimica Acta* **1984**, *161*, 275.

109. Zhang, X.; Duan, Y.; He, L.; Li, D.; Zhou, J.; Yu, R.; Shen, W.; Zhao, S.; Shuyun, G.; Zhang, S. *Guangpuxue Yu Guangpu Fenxi* **1992**, *12*, 99.
110. Carr, J.J. *Elements of Microwave Technology*; Harcourt Brace Jovanovich: Orlando, FL, 1989; p. 212.
111. Okress, E.C. *Handbook of Microwave Measurements*, Volume 1; Wind, M.; Rapaport, H., Editors; Polytechnic Press: Brooklyn, NY, 1955; p. 18-1.
112. Southworth, G.C. *Principles and Applications of Waveguide Transmission*; D. Van Nostrand: Princeton, NJ, 1956; p. 572.
113. Sarbacher, R.I.; Edson, W.A. *Hyper and Ultrahigh Frequency Engineering*; John Wiley and Sons: New York, NY, 1943; p. 552.
114. Brandenberger, J.R. *Review of Scientific Instrumentation* **1971**, *42*, 1535.
115. Ragan, G.L. *Microwave Transmission Circuits*; McGraw-Hill: New York, NY, 1948; p. 26.
116. Schelkunoff, S.A. *Electromagnetic Waves*; D. Van Nostrand: Princeton, NJ, 1960; p. 242.
117. Adam, S.F. *Microwave Theory and Applications*; Prentice-Hall: Englewood Cliffs, NJ, 1969; p. 51.
118. Slater, J.C. *Microwave Electronics*; D. Van Nostrand: Princeton, NJ, 1959; p. 1.
119. Ali, A. H.; Winefordner, J. D. *Analytica Chimica Acta* **1992**, *264*, 327.
120. Meiners, L.G.; Alford, D.B. *Review of Scientific Instrumentation* **1986**, *57*, 164.
121. Chilukuri, S.; Lichten, W.L. *Review of Scientific Instrumentation* **1979**, *50*, 256.
122. Ingle, Jr., J.D.; Crouch, S.R. *Spectrochemical Analysis*; Prentice-Hall: Englewood Cliffs, NJ, 1988; p. 115.
123. Malmstadt, H.V.; Enke, C.G.; Crouch, S.R. *Electronics and Instrumentation for Scientists*; Benjamin/Cummings Publishing: Menlo Park, CA, 1981; p. 114.
124. Ali, A.H.; Ng, K.C.; Winefordner, J.D. *Journal of Analytical Atomic Spectrometry* **1991**, *6*, 211.
125. Carr, J.J. *Elements of Microwave Electronics Technology*; Harcourt, Brace, Jovanovich: New York, NY, 1989; p. 187.

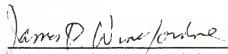
126. Vermaak, H.; Kujirai, O.; Hanamura, S.; Winefordner, J.D. *Canadian Journal of Spectroscopy* **1986**, *31*, 95.
127. Ali, A.H.; Winefordner, J. D. *Analytica Chimica Acta* **1992**, *264*, 319.
128. Pearse, R.W.B.; Gaydon, A.G. *The Identification of Molecular Spectra*, 4<sup>th</sup> ed.; John Wiley & Sons: New York, NY, 1976.
129. Horlick, G. *Applied Spectroscopy* **1976**, *30*, 113.
130. *Varian Guide to ICP/AAS analytical values* (PN 85 101009 00).
131. Urh, J.J.; Carnahan, J.W. *Analytical Chemistry* **1985**, *57*, 1253.
132. Alvarado, J.; Carnahan, J.W. *Applied Spectroscopy* **1993**, *47*, 2036.
133. Haas, D.L.; Caruso, J.A. *Analytical Chemistry* **1984**, *56*, 2014.
134. Patel, B.M.; Deavor, J.P.; Winefordner, J.D. *Talanta* **1988**, *35*, 641.
135. Zhang, Y.K.; Hanamura, S.; Winefordner, J.D. *Applied Spectroscopy* **1985**, *39*, 226.
136. Chan, W.T.; Horlick, G. *Applied Spectroscopy* **1990**, *44*, 380.
137. Alvarado, J.; Cavalli, P.; Omenetto, N.; Rossi, G. *Analytical Letters* **1989**, *22*, 2975.
138. Heltai, G.Y.; Broekaert, J.A.C.; Burba, P.; Leis, F.; Tschopel, P.; Tolg, G. *Spectrochimica Acta* **1990**, *45B*, 857.
139. Kreiger, J. *Chemical and Engineering News* **1992**, *70*, 27.
140. O'Haver, T.C. *Analytical Chemistry* **1979**, *51*, 91A.
141. Savitzky, A.; Golay, M. *Analytical Chemistry* **1964**, *36*, 1628.
142. Parsons, P.J.; Slavin, W. *Spectrochimica Acta* **1993**, *48B*, 925.
143. Ali, A.H.; Ng, K.C.; Winefordner, J.D. *Spectrochimica Acta* **1991**, *46B*, 1207.

## BIOGRAPHICAL SKETCH

Michael was born in Jamestown, NY, in 1967. He graduated from Conestoga Senior High School, Berwyn, PA, in 1985, and proceeded directly to Virginia Tech, Blacksburg, VA. He received his Bachelor of Science in chemistry in 1989, aided by a four-year DuPont Scholarship. He then was hired by DuPont Corporation, where he served as an Analytical Chemist for three months, prior to entering graduate school at the University of Florida in 1989. He majored in analytical chemistry and conducted research under the supervision of Dr. James D. Winefordner. Specifically, Michael characterized diode lasers for their use in atomic spectroscopy and a capacitively coupled microwave plasma for the determination of lead in whole blood. He received his Ph.D. from the University of Florida in August 1994. His next project lies at the Army Research Lab, Aberdeen, MD, where he will be funded by a National Research Council Postdoctoral Fellowship.

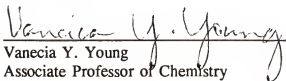


I certify that I have read this study and that in my opinion it conforms to acceptable standards of scholarly presentation and is fully adequate, in scope and quality, as a dissertation for the degree of Doctor of Philosophy.



James D. Winefordner, Chair  
Graduate Research Professor of Chemistry

I certify that I have read this study and that in my opinion it conforms to acceptable standards of scholarly presentation and is fully adequate, in scope and quality, as a dissertation for the degree of Doctor of Philosophy.



Vanecia Y. Young  
Associate Professor of Chemistry

I certify that I have read this study and that in my opinion it conforms to acceptable standards of scholarly presentation and is fully adequate, in scope and quality, as a dissertation for the degree of Doctor of Philosophy.



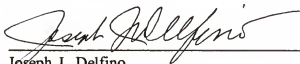
Richard Yost  
Professor of Chemistry

I certify that I have read this study and that in my opinion it conforms to acceptable standards of scholarly presentation and is fully adequate, in scope and quality, as a dissertation for the degree of Doctor of Philosophy.



David Richardson  
Associate Professor of Chemistry

I certify that I have read this study and that in my opinion it conforms to acceptable standards of scholarly presentation and is fully adequate, in scope and quality, as a dissertation for the degree of Doctor of Philosophy.



Joseph J. Delfino  
Professor of Environmental  
Engineering Sciences

This dissertation was submitted to the Graduate Faculty of the Department of Chemistry in the College of Liberal Arts and Sciences to the Graduate School and was accepted as partial fulfillment of the requirements for the degree of Doctor of Philosophy.

August 1994

---

Dean, Graduate School